

Chapter 4

Characteristics and Formation of the Jerónimo Carbonate-Replacement Gold Deposit, Potrerillos District, Chile

JOHN F. H. THOMPSON,[†]

Teck Cominco Limited, 200 Burrard Street, Vancouver, British Columbia, Canada V6C 3L9

VANESSA G. GALE,* RICHARD M. TOSDAL,

Mineral Deposit Research Unit, Department of Earth and Ocean Sciences, University of British Columbia, Vancouver, British Columbia, Canada V6T 1Z4

AND WILLIAM A. WRIGHT

Barrick Gold Corporation, 3165 Susileen Drive, Reno, Nevada 89590

Abstract

The Jerónimo sedimentary rock-hosted disseminated Au deposit is located within the Potrerillos district of the Atacama region of northern Chile, east of the Potrerillos porphyry Cu-Mo and El Hueso high-sulfidation Au deposits. Prior to development, the Jerónimo deposit contained a resource of approximately 16.5 million metric tons (Mt) at 6.0 g/t Au. Production began in the oxidized, nonrefractory portion of the deposit in 1997 and terminated in 2002. During that time, approximately 1.5 Mt at 6.8 g/t Au was mined by underground room-and-pillar methods, from which a total of approximately 220,000 oz of Au was recovered by heap-leach cyanidation.

Jerónimo mineralization occurs as irregular strata-bound lenses within particular bioclastic limestone units of the Jurassic Asientos Formation. The manto-shaped mineralized zone extends over an area of approximately 2.0 by 1.3 km and averages 6 m in thickness. Mineralization and alteration are focused along subvertical fractures and joints within the bioclastic units. Alteration involved decarbonatization followed by the formation of the following assemblages: (1) intense, pervasive, replacement-style silicification; (2) carbonate, mainly restricted to vugs, consisting of Mn carbonate (rhodochrosite and kutnohorite) in the center of the orebody and calcite-dolomite on the margins; and (3) argillization, consisting of illite as widespread disseminations and veinlets and kaolinite as vug fillings in the center of the deposit. Other common alteration minerals include apatite, rutile, monazite, and barite. The ore mineral suite consists of pyrite, arsenopyrite, sphalerite, lead sulfosalts, orpiment, and realgar, with minor coloradoite, altaite, cinnabar, and cassiterite. Gold is present dominantly as submicron-sized grains, ranging from 140 nm to 1.13 μm , that are encapsulated in pyrite, arsenopyrite, quartz, and realgar and also occur within vugs in the silicified matrix.

Lead isotope results of the main-stage sulfide and sulfosalt minerals ($^{206}\text{Pb}/^{204}\text{Pb}$: 18.564–18.644; $^{207}\text{Pb}/^{204}\text{Pb}$: 15.592–15.662; $^{208}\text{Pb}/^{204}\text{Pb}$: 38.536–38.638) indicate that lead in the ore fluids was dominantly from a Tertiary magmatic source, with input from a more radiogenic source—igneous Carboniferous to Triassic basement rocks and/or the overlying Jurassic limestone and sandstone. Carbon and oxygen isotope compositions of ore zone rhodochrosite and kutnohorite, ranging from $\delta^{18}\text{O}$ of 16.65 to 22.52 per mil (VSMOW) and $\delta^{13}\text{C}$ of –2.84 to –1.3 per mil (PDB), suggest contributions from both magmatic and Jurassic limestone wall-rock sources.

The critical features that define the style of mineralization at Jerónimo include lithological and structural control, enrichment in Au-As-Mn-Zn-Pb-Ag-Hg, silicification and carbonate alteration, the presence of native Au grains, the close spatial association with porphyry and related styles of mineralization, and isotopic evidence for a magmatic contribution to metals and hydrothermal fluids. These characteristics are more similar to carbonate-replacement deposits than to typical Carlin-type sediment-hosted Au deposits. Structural and isotopic data suggest that Jerónimo is late Eocene-early Oligocene in age, but the precise temporal and genetic relationships of Jerónimo to other magmatic-hydrothermal systems in the district are unknown.

Resumen

El depósito de oro hospedado en rocas sedimentarias de Jerónimo se ubica en el distrito de Potrerillos, Región de Atacama, norte de Chile, al este del pórfido de Cu-Mo de Potrerillos y del depósito de alta sulfidación de El Hueso. Al inicio de su desarrollo, Jerónimo contenía un recurso aproximado de 16,5 millones de toneladas métricas con una ley de 6,0 g/t Au. La producción comenzó en la parte oxidada, no refractaria, del depósito en 1997 y culminó en el año 2002. Durante este período se extrajo, por el método de cámaras y pilares, aproximadamente 1,5 millones de toneladas métricas con una ley de 6,8 g/t Au, para una producción acumulada de aproximadamente 200.000 onzas de Au, las que fueron recuperadas mediante el método de cianuración en pilas.

[†] Corresponding author: e-mail, john.thompson@teckcominco.com

* Present address: Les Fougères, 783 Route 105, Chelsea, Quebec, Canada J9B 1P1.

La mineralización de Jerónimo se presenta como lentes estrato-ligados irregulares dentro de ciertos horizontes de caliza bioclástica de la Formación Asientos, de edad jurásica. La zona mineralizada, con forma de manto, se extiende sobre un área de aproximadamente 2,0 por 1,3 km y posee un espesor promedio de 6 m. La alteración y la mineralización están controladas por fracturas subverticales presentes dentro de los niveles bioclásticos. La alteración involucró un proceso de decarbonatización inicial de la roca de caja, el que fue seguido por la formación sucesiva de los siguientes ensamblajes: (1) silicificación pervasiva, de tipo reemplazo; (2) carbonatos de manganeso (rodocrosita y kutnohorita) en el centro del depósito y calcita-dolomita en sus bordes; y (3) argilización, con illita en forma diseminada y en vetillas y, caolinita, como relleno de espacios abiertos en la parte central del depósito. Otros minerales de alteración comunes corresponden a apatito, rutilo, monazita y baritina. La mineralogía de mena está constituida por pirita, arsenopirita, esfalerita, sulfosales de plomo, oropimente y rejalgá, además de cantidades subordinadas de coloradoita, altaíta, cinabrio y casiterita. El oro se encuentra, predominantemente, en granos de tamaño submicrón, entre 140nm y 1,13 μm , los que están encapsulados en pirita, arsenopirita, cuarzo y rejalgá. Granos de oro de tamaño similar, localizados en espacios abiertos de la matriz silicificada de la roca, son también comunes.

Los resultados de los isótopos de plomo del estadio principal de sulfuros y sulfosales ($^{206}\text{Pb}/^{204}\text{Pb}$: 18,564 a 18,644; $^{207}\text{Pb}/^{204}\text{Pb}$: 15,592 a 15,662; y $^{208}\text{Pb}/^{204}\text{Pb}$: 38,536 a 38,638) indican que el plomo en los fluidos mineralizantes tuvo, principalmente, una fuente magmática de edad terciaria, además de cierta participación menor de una fuente algo más radiogénica (basamento Carbonífero-Triásico ígneo y/o caliza y arenisca jurásicas sobreyacentes). Los isótopos de carbono y oxígeno de rodocrosita y kutnohorita de la zona de mena presentan un rango de $\delta^{18}\text{O}$ entre 16,65 y 22,52 per mil (VSMOW) y de $\delta^{13}\text{C}$ entre -2,84 a -1,30 per mil (PDB) y sugieren contribuciones desde fuentes magmáticas y de la caliza jurásica hospedante.

Las características críticas que definen el estilo de mineralización en Jerónimo incluyen el control estructural y litológico sobre la mineralización, su enriquecimiento en Au-As-Mn-Pb-Ag-Hg, la alteración carbonatada y silicificación, la presencia de granos de oro nativo, la relación espacial con mineralización tipo pórfido y otros estilos relacionados y, la evidencia isotópica sobre una contribución magmática en los metales y fluidos hidrotermales. Estas características son más parecidas a las de los depósitos de reemplazo en rocas carbonatadas que a aquellos depósitos de tipo Carlin típicos, estos últimos con oro hospedado en rocas sedimentarias. Aunque los antecedentes estructurales e isotópicos sugieren una edad eocena-oligocena para Jerónimo, sus relaciones temporales y genéticas con otros sistemas magmático-hidrotermales del distrito permanecen aún desconocidas.

Introduction

THE ROLE of magmatism in the formation of sedimentary rock-hosted disseminated Au deposits has been widely debated. The spatial, and in some cases, temporal association between sediment-hosted Au deposits and granitic intrusive complexes suggests a direct genetic link (e.g., Sillitoe and Bonham, 1990; Theodore, 2000), but in other cases the spatially associated intrusion differs significantly from the age assigned to mineralization and no immediate relationship can be defined (Hofstra and Cline, 2000). Isotopic studies on several deposits suggest that ore fluids were dominated by evolved meteoric water although other fluid sources (metamorphic and magmatic) are not necessarily ruled out (e.g., Radtke et al., 1980; Ilchik, 1990; Hofstra and Cline, 2000; Cline et al., 2003). In an attempt to rationalize apparent differing relationships to intrusions, Hofstra and Cline (2000) divided sediment-hosted Au deposits into two end members, Carlin-type and distal-disseminated where the latter are interpreted to have a direct relationship to intrusions.

A broad family of mineral deposits that form by replacement of carbonate-rich rocks in the distal parts of intrusion-centered, magmatic-hydrothermal systems has been recognized for many years (e.g., Prescott, 1926; Megaw et al., 1988; Beaty et al., 1990; Megaw, 1998). These carbonate-replacement deposits contain a variable metal suite that may include Cu, Zn, Pb, Ag, and Au with local enrichment in other trace elements (W, Sn, Bi, Mn, As, Sb, Te, and Hg). Gold-rich, base metal-poor deposits have been recognized as a distinct end member of the carbonate-replacement deposits and are interpreted to form in the more distal parts of magmatic-hydrothermal systems (Sillitoe and Bonham, 1990; Sillitoe, 1991a).

Gold-rich carbonate-replacement deposits share a number of characteristics with Carlin-type deposits, including strong lithologic and structural controls, host rocks, and alteration types (decarbonatization, silicification, and argillization). Although Au is fine grained in both types of deposit, the precise mineralogical controls on the distribution of gold, and the mineralogy and related geochemistry may differ substantially between them. The extent to which this reflects different fluid and metal sources, different mineralizing processes, or varying distances from the center of the system is yet to be proven on a specific deposit by deposit basis.

The Jerónimo gold deposit is located in the Potrerillos district (26°30' S, 69°24' W) of the Atacama region of northern Chile, approximately 50 km south of El Salvador (Fig. 1). Jerónimo comprises zones of both oxide and sulfide Au mineralization. The oxide zone was discovered in 1994 and the sulfide portion of the deposit was found the following year. The oxide deposit was placed in production in 1997 by Agua de la Falda S.A., a joint venture between Minera Homestake Chile S.A. and the Corporación Nacional del Cobre (Codelco), and was worked out in 2002. Prior to development, the combined oxide-sulfide Jerónimo deposit contained a resource of approximately 16.5 million metric tons (Mt) at 6.0 g/t Au. Underground room-and-pillar mining of the oxide zone produced approximately 1.5 Mt at 6.8 g/t Au, from which a total of approximately 45,000 oz of Au was recovered annually by heap-leach cyanidation (Homestake Mining Company Annual Report, 2000).

The Potrerillos district is best known for porphyry Cu-Mo-(Au) mineralization at Potrerillos, mined until 1959, and sedimentary- and volcanic rock-hosted disseminated Au at El Hueso, mined between 1986 and 1995. Marsh (1997) dated a

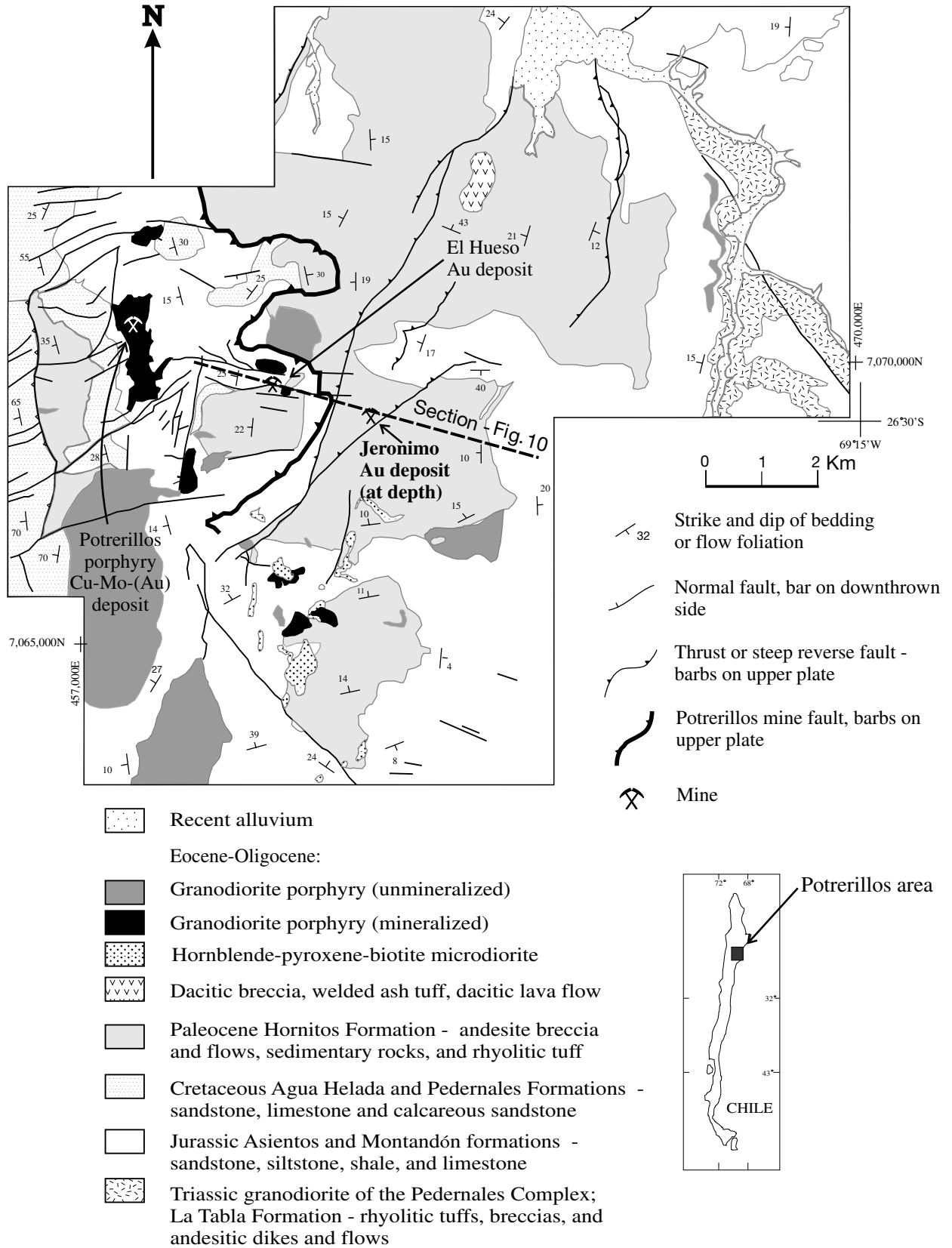


FIG. 1. Geologic map of the Potrerillos district, showing the location of the Cobre porphyry and contained Potrerillos porphyry Cu-Mo-(Au) deposit, the El Hueso Au deposit, and the Jerónimo Au deposit (modified after Marsh, 1997). Inset shows location of the area in Chile. Line of section for Figure 10 is shown.

variety of primary igneous and secondary alteration minerals by high-resolution Ar-Ar methods to evaluate the relationship among Potrerillos, El Hueso, and other intrusive bodies in the district. Marsh (1997) and Marsh et al. (1997) determined that El Hueso formed between 40.2 and 40.8 Ma, prior to the Potrerillos porphyry Cu mineralization, which occurred between 35.6 and 35.9 Ma, apparently discounting the possibility of the immediate genetic link proposed by Sillitoe (1991b). The result of this work implies that an extended period of magmatic and magmatic-hydrothermal activity occurred in the Potrerillos district, with the existence of at least two spatially distinct magmatic-hydrothermal systems.

The purpose of the study described herein was to determine the style of mineralization in the Jerónimo deposit, the major controls on mineralization, and the potential relationship to the other deposits in the Potrerillos district. Detailed mineralogic studies combined with initial Pb, C, and O isotope analyses indicate that Jerónimo is a Au-rich carbonate-replacement deposit that most likely formed from fluid moving through fault systems in the footwall of the deposit. The relationship of Jerónimo to the other deposits in the district is still poorly constrained.

Regional Setting

Crystalline basement in northern Chile, in the vicinity of Potrerillos, consists of late Paleozoic-Triassic plutonic, metavolcanic, and metasedimentary rocks (Cornejo et al., 1993). In the Middle Jurassic to early Late Cretaceous, a magmatic arc was active and is now exposed in the Coastal Cordillera of northern Chile and southern Peru. In northern Chile, the arc was accompanied by the opening of the Tarapacá back-arc basin in which several thousand meters of carbonate and siliciclastic sediments were deposited (Mpodozis and Ramos, 1990). Between 100 and 80 Ma, the onset of sea-floor spreading in the South Atlantic and subsequent increase in the rate of westward motion of the South American plate resulted in the collapse, closure, and uplift of the Tarapacá basin (Mpodozis and Ramos, 1990; Davidson and Mpodozis, 1991).

Following a lull during the Late Cretaceous, calc-alkaline magmatism resumed during the Paleocene in northern Chile. The foci of arc magmatism continued to migrate eastward during the Tertiary, producing progressively younger arcs to the east (Davidson and Mpodozis, 1991). Oblique convergence of the Nazca and South American plates induced strike-slip motion, forming the regional north-striking Domeyko fault system. At the end of oblique convergence, during the late Eocene to early Oligocene, the most significant porphyry copper deposits in northern Chile were emplaced syntectonically along transpressional structures within the Domeyko fault system (Davidson and Mpodozis, 1991; Tomlinson et al., 1994). Potrerillos is one of the most southerly deposits in the late Eocene-early Oligocene belt.

Potrerillos District Geology

Pre-Jurassic basement units in the Potrerillos district include Carboniferous to Triassic granite, diorite, tonalite, and quartz syenite, metavolcanic rocks, and minor quartz-muscovite schist (Olson, 1983). During the Jurassic, sedimentation in the Tarapacá back-arc basin resulted in the deposition

of calcareous mudstone and limestone of the Montandón Formation on the pre-Jurassic basement (Olson, 1983). This formation grades upward into the mixed carbonate and clastic sedimentary rocks of the Asientos Formation, which hosts the Jerónimo deposit, and is conformably overlain by siltstone and limestone of the Late Jurassic to Early Cretaceous Pedernales Formation (Fig. 2).

In the Potrerillos district, Eocene to Oligocene transpression, linked to deformation along the Domeyko fault system, was manifested as asymmetric folding and thrust and reverse faulting, which formed the Potrerillos fold and thrust belt (Cornejo et al., 1993). The dominant structure produced by this deformation is the Potrerillos Mine fault, an east-south-east-vergent thrust fault with approximately 1.5 km of displacement (Tomlinson et al., 1994). The Cobre porphyry, which hosts the Potrerillos porphyry Cu-Mo-(Au) deposit, was emplaced syntectonically with movement along this fault (Mpodozis et al., 1994; Tomlinson, 1994). The Potrerillos porphyry deposit and the El Hueso Au deposit are both located in the upper plate of the Potrerillos Mine fault. Porphyry-type mineralization, possibly the part of the Potrerillos system, occurs below the fault 1.5 km west of the Potrerillos mine (Tomlinson, 1994; Marsh, 1997), and the Jerónimo deposit is also located in the footwall of the fault, 1.5 km to the east of El Hueso (Fig. 1). More than ten granodioritic, quartz monzodioritic, and tonalitic plagioclase-porphyrific intrusions were emplaced in the Potrerillos district from the late Eocene to early Oligocene, between 40.8 and 32.6 Ma (Marsh, 1997; Marsh et al., 1997).

Economic mineralization in the Potrerillos porphyry deposit is largely restricted to the Cobre porphyry, but skarns and related contact metamorphism formed in the surrounding Montandón, Asientos, and Pedernales Formations (Olson, 1983). Mantolike bodies hosting Cu mineralization occur in limestone horizons within the Asientos Formation. More distal alteration extending away from the Cobre porphyry consists of disseminated pyrite and secondary actinolite in sandy lithologies and pyroxene-garnet-quartz-anhydrite-calcite skarn-hornfels grading outward to pyrite-sphalerite in thermally metamorphosed marls and impure carbonate rocks. The latter extend up to 1,500 m from the Cobre porphyry. Pure limestone horizons are silicified within 900 m of the contact.

The Au deposit at El Hueso consists of replacement-style mineralization focused in steep, east-west trending faults and adjacent porous, gently dipping bioclastic limestone beds, particularly unit G of the Asientos Formation (Fig. 2). Faulting is interpreted to be premineral, related to early Tertiary compression (Tomlinson, 1994). The deposit is truncated at depth by the Potrerillos Mine fault, however, unlike the Potrerillos porphyry deposit no evidence for synmineralization movement is identified at El Hueso (Marsh, 1997). Alteration is dominated by silicification in porous lithologies and banded or spotted ("moteada") quartz-illite assemblages in less porous rocks. Postmineralization advanced argillic alteration (alunite, pyrophyllite, zunyite, dickite, woodhouseite, rutile, diaspore, quartz) occurs in crosscutting veins related to steep faults. Hypogene alunite returned a $^{40}\text{Ar}/^{39}\text{Ar}$ date of 36.23 ± 0.07 Ma (Marsh, 1997; Marsh et al., 1997), significantly younger than the age of sericite related to Au

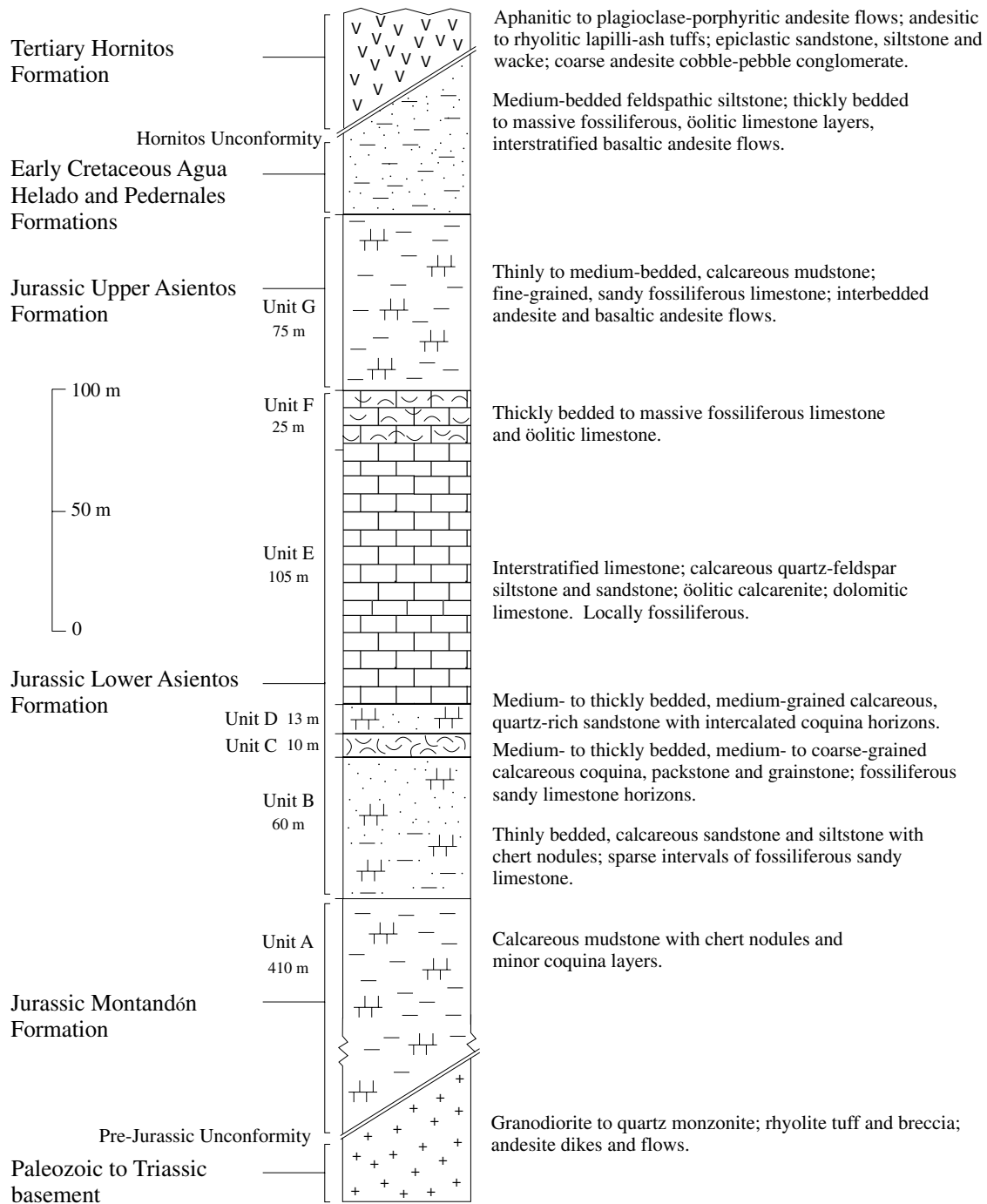


FIG. 2. Generalized stratigraphic column for Mesozoic and Tertiary units in the Potrerillos-Jerónimo area (modified from Marsh, 1997).

mineralization (40.25 ± 0.05 Ma; Marsh, 1997; Marsh et al., 1997) but similar to the age of the Cobre porphyry and its contained porphyry Cu mineralization. The advanced argillic alteration may represent the remnants of a district-wide lithocap related to the Potrerillos porphyry Cu deposit (Sillitoe, 1997).

Geology of the Jerónimo Deposit

The eastern edge of the oxide part of the Jerónimo deposit was exposed in sparse outcrops. The majority of the deposit,

however, lies at depths of 100 to 600 m below surface where drilling has defined a mantolike body that dips gently to the northwest and averages 6 m thick. In plan, the deposit has an oval shape, based on a 1 g/t Au cutoff, covering an area of approximately 2 by 1.3 km (Fig. 3). The sulfide part of the deposit, the focus of this study, is subdivided into two zones referred to as upper and lower Jerónimo (Figs. 3–4). The two zones are separated by the north- to northwest-striking Polvorines and the variable east- to northeast-striking

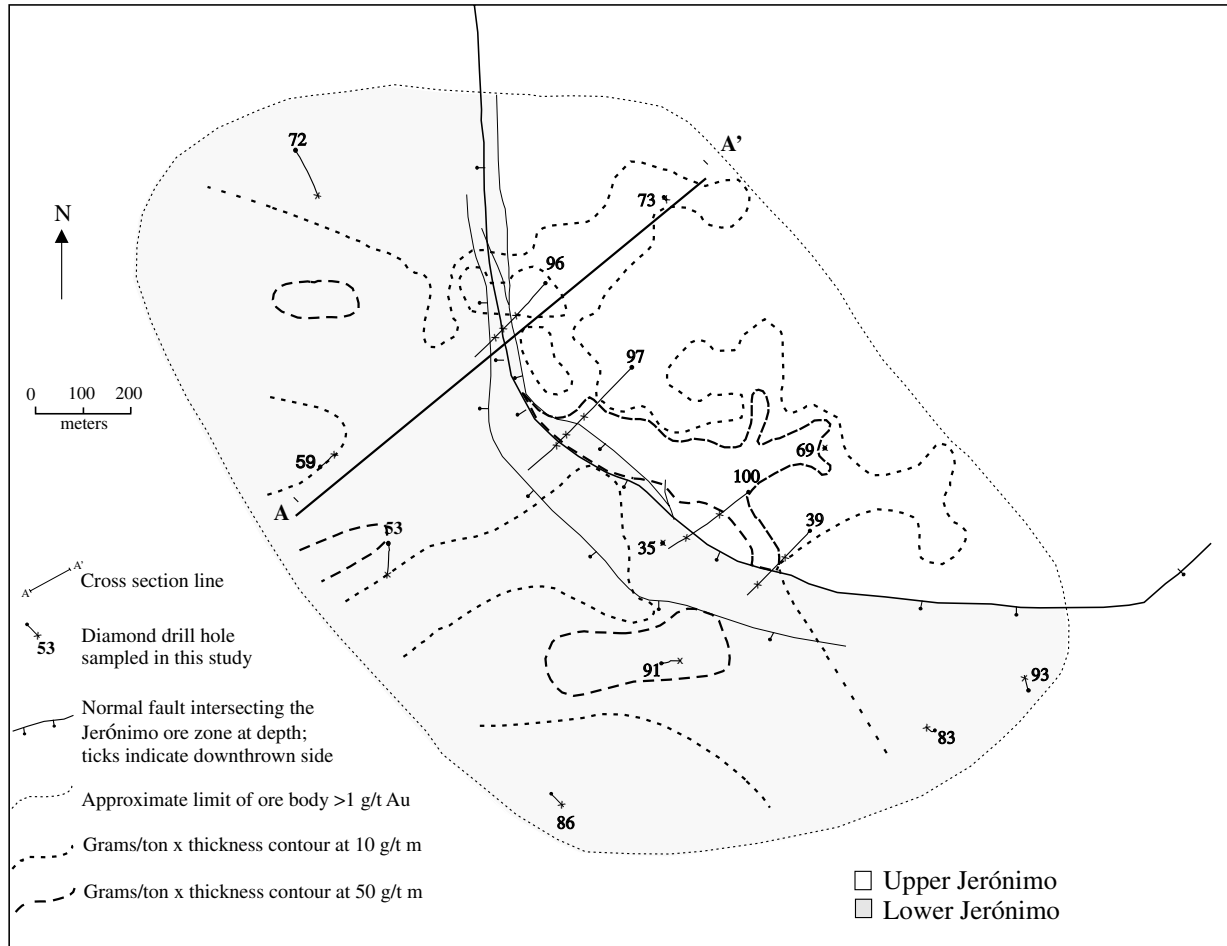


FIG. 3. Plan view of the Jerónimo upper and lower sulfide body, approximately outlined by the 1-g/t Au contour. The distribution of the better intervals of Au mineralization is indicated by grade-tonnage contours based on all data and work by Minera Homestake Chile. Section A-A' shown in Figure 4.

Mapuche fault systems that link together in the Jerónimo area to drop the host limestone beds to the south, west, and east by as much as 400 m in a series of steps (Fig. 4). The fault systems also influenced the deposition of early Tertiary volcanoclastic rocks (Lazcano and Fuentes, 1997) and are therefore premineral. Assay results of core from inclined diamond drill holes that pierced the subvertical Mapuche fault show that Au grades are locally elevated within the fault zone (e.g., 2.9 g/t), suggesting that it acted as one of the conduits for mineralizing fluid.

Elgueta and Fuentes (1997) recognized two cycles of transgression and regression represented by the Montandon and Lower Asientos Formations and the Upper Asientos and Pedernales Formations, respectively (Fig. 2). The result is a sequence of lithologies that vary from calcareous sandstone, siltstone, and mudstone to oölitic and bioclastic limestone. Recognition of the lithologic control on mineralization at Jerónimo led to detailed stratigraphic mapping and subdivision of the Asientos Formation into seven distinct units (Dilles, 1995; Fig. 2). The majority of the Jerónimo deposit is hosted by unit C and adjacent parts of unit B below and unit D above. The dominant lithologic host is poorly sorted

bioclastic limestone with large, typically 8- by 4-mm, pelecypod and gastropod shells. This limestone generally consists of 30 vol percent bioclasts, 50 vol percent coated carbonate grains, and 20 vol percent calcite spar cement, with as much as 4 vol percent subangular detrital quartz grains, typically 0.3 by 0.2 mm in size. A second ore-hosting lithology is a fossiliferous sandy limestone. It is moderately sorted and generally consists of 70 vol percent bioclasts, 10 vol percent intraclasts, and 20 vol percent spar cement, with rare fine-grained detrital quartz grains. Bryozoan mat fragments ranging from 0.5 to 0.7 mm in size comprise the dominant bioclast type and are generally subangular to subrounded, spherical, and have a porous texture. In contrast, lithologic units in the Asientos Formation that do not host ore are poorly to moderately sorted, matrix-supported, sandy limestone. These consist of 10 to 50 vol percent quartz grains and less than 70 vol percent calcite allochems, with minor small bioclasts, typically 0.7 by 0.2 mm. The matrix of the sandy limestone may consist of spar or secondary chalcedony and clay.

Caddey (1999) identified a set of late subvertical faults with centimeter-scale offsets, which crosscut the ore-hosting bioclastic beds, overlying units, and some thrust faults, and

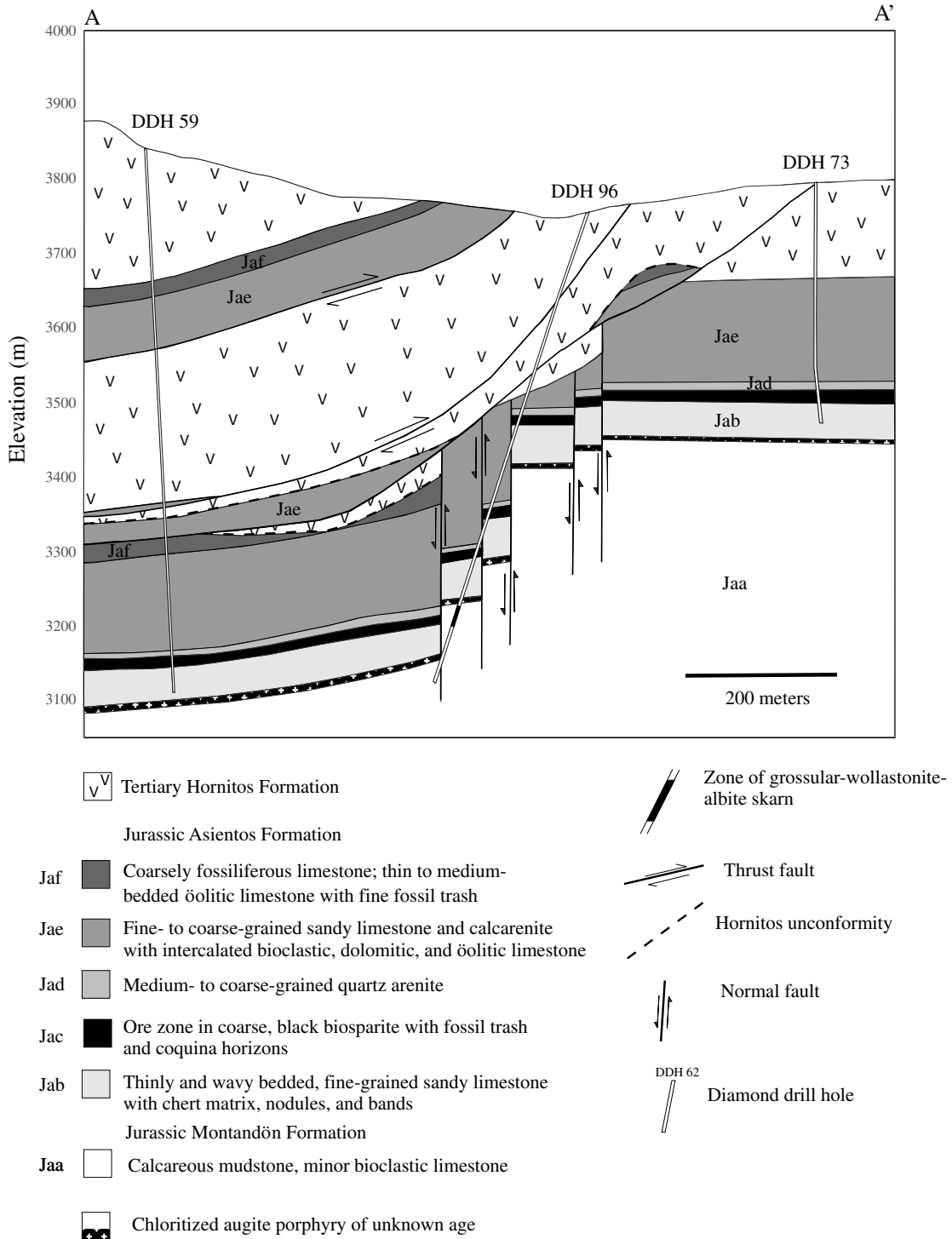


FIG. 4. Cross section through the Jerónimo sulfide body, showing major lithologic units and the fault system that divides the deposit in unit C (Jac) into upper and lower parts.

host calcite and As sulfide minerals. Caddey (1999) also observed that the bioclastic limestone beds contain fractures and joints that host Mn carbonate, quartz, pyrite, and As sulfide minerals. Caddey (1999) interpreted the faults, fractures, and joints to be premineral, probably having formed during or immediately after early Tertiary folding, thrusting,

and reverse faulting. Major faults may have acted as feeders (Caddey, 1999; Simian, 2000), channeling ore fluid to the bioclastic horizons, as indicated by local gold mineralization in the Mapuche fault. In addition, structural preparation of the bioclastic limestone may have enhanced the porosity and permeability.

Alteration

Hypogene alteration in the Jerónimo deposit and the relationship of alteration to lithology and Au grade were evaluated by detailed logging and sampling of 14 drill holes through the Jerónimo deposit (Gale, 1999; Fig. 3). Alteration is dominated by silicification, carbonatization, and argillization. The limestone protolith within the ore zone was completely decarbonated prior to and during silicification and the introduction of secondary carbonate. A narrow zone of skarn (grossular-wollastonite-albite) was identified in the calcareous mudstone of unit A in one hole below the ore zone (Fig. 4).

Decarbonatization-silicification

Complete decarbonatization encompasses all alteration and associated mineralization. In the mineralized zone, the limestone is completely silicified, but locally vuggy textures suggest decarbonatization and partial bulk dissolution of the limestone prior to or during silicification. Partial decarbonatization-silicification resulting in vuggy limestone extends above and below the altered and mineralized horizon (Gale, 1999).

Secondary quartz is the most abundant mineral in the ore zone, comprising between 5 and 90 vol percent of the host lithology. Silicification is characterized by replacement-style quartz that occurs as fine-grained anhedral intergrown grains. The secondary quartz commonly preserves fossil shapes and textures. Pelecypod clasts, generally ranging from 2 by 0.5 to 10 by 1 mm, are replaced either by equant, interlocking quartz grains or by elongate, anhedral fibrous quartz. The delicate porous texture of the bryozoan mats is also locally preserved. The centers of the silicified pelecypod clasts are typically vuggy, lined with drusy quartz, and may be filled by carbonate minerals. Minerals that occur as grains intergrown with quartz include pyrite, arsenopyrite, sphalerite, apatite, rutile, monazite, and barite. Apatite also occurs as well-rounded

grains similar to detrital intraclasts in the unaltered host rocks and may therefore be partially premineral. Rutile is associated with pyrite, both being disseminated in the quartz. Barite forms large subhedral grains and diffuse aggregates within quartz and locally fills vugs. Micron-scale grains of La-Ce-Nd-bearing monazite occur as inclusions in quartz and within vugs.

Carbonatization

Primary or diagenetic carbonate minerals within the Asientos Formation consist of pure calcite, dolomite, or locally ferroan dolomite, with only trace Mn (Gale, 1999; Simian, 2000). In contrast, secondary hydrothermal carbonates within the ore zone are dominated by rhodochrosite and kutnohorite. Secondary Mn-rich carbonate minerals form an elliptical, northwest-trending zone, with an area of approximately 1.6 by 0.8 km, overlapping the center of the orebody (Fig. 5). Hydrothermal calcite forms a 200-m-wide zone that surrounds the Mn carbonate zone.

The Mn carbonate and silicate minerals were identified by petrography, X-ray diffraction (XRD), and electron microprobe analysis (Gale, 1999). Manganese minerals typically comprise between 0 and 20 vol percent of the alteration mineralogy in the core of the deposit but locally form up to 70 vol percent. Kutnohorite occurs as subhedral grains, locally intergrown with rhodonite, typically rimming or filling vugs in the silicified matrix or within the vuggy centers of silicified bioclasts. Kutnohorite also occurs as fine-grained massive aggregates, disseminated grains, and irregular veinlets that range in width from 25 to 175 μm and crosscut the quartz matrix. The distribution of light pink rhodochrosite is erratic, occurring in thin, typically <4-mm, irregular veinlets. The Mn carbonate aggregates host inclusions of pyrite, sphalerite, rutile, monazite, rhodonite, and barite. Calcite enriched in rare earth elements (La, Ce, Nd) is present in some strongly silicified samples as dendritic crystals within aggregates typically 4 by 0.5 μm in size. Like the Mn carbonate minerals, calcite

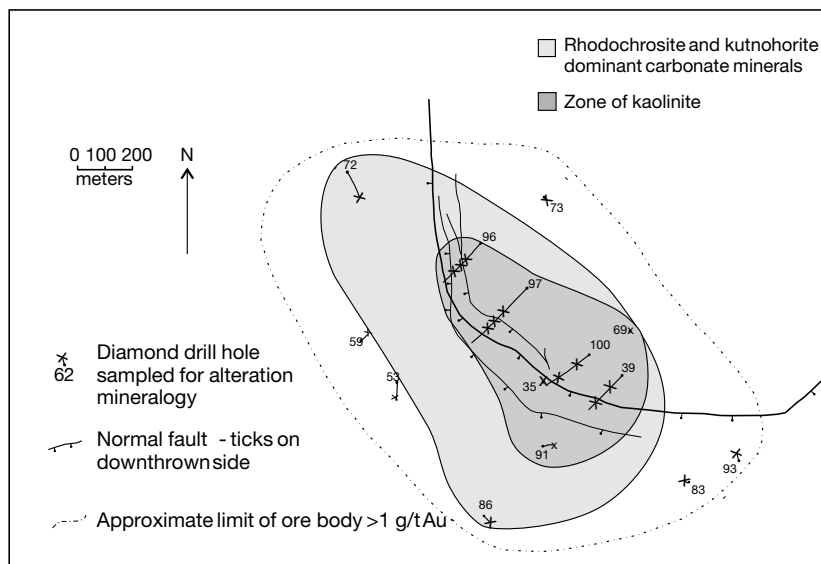


FIG. 5. Plan view of the mineralized horizon projected to surface, showing carbonate and clay mineral alteration zoning. The approximate outline of mineralization is shown by the 1-g/t Au contour.

occurs in the outer part of the Jerónimo deposit, filling open spaces at the center of silicified bioclasts. Additionally, calcite occurs in late, irregular veinlets hosting orpiment, realgar, and minor cinnabar.

Electron microprobe analyses of the carbonates (Gale, 1999; Fig. 6) indicate that compositions are relatively homogeneous in individual samples, but that there is extensive variation in the Mn/Fe ratio forming a fairly complete solid solution between rhodochrosite and siderite. The dolomite group minerals also show solid solution between kutnohorite and more Mg rich compositions. Two samples contain kutnohorite with appreciable Fe (Fig. 6).

Argillization

Clay minerals typically comprise 10 vol percent of the ore but may form up to 60 vol percent. Clay minerals were identified largely by XRD supported by the use of PIMA (short wave infrared reflectance (SWIR) spectrometer) to evaluate illite crystallinity and to differentiate kaolinite from dickite (Gale, 1999). Illite occurs throughout the deposit, while kaolinite is restricted to an elliptical zone approximately 1.0 by 0.5 km in size in its center (Fig. 5).

Illite occurs in three textural forms: (1) finely disseminated within the silicified matrix; (2) in patches and anastomosing bands, typically 2 mm wide, and in rare, irregular, discontinuous veinlets, averaging approximately 120 μm in width, that crosscut the silicified matrix; and (3) filling vugs within aggregates of carbonate and quartz. Illite-filled vugs locally host grains of pyrite, arsenopyrite, galena, sphalerite, coloradoite, cassiterite, rutile, native Au, barite, monazite, and apatite. Rare alumino-phosphate-sulfate (APS) minerals (svanbergite and woodhouseite) are present in some illite-filled vugs where apatite is absent, possibly reflecting local replacement of apatite during argillic alteration. Analysis of illite by XRD and SWIR indicates that minor (<10%) smectite interlayering is present (Gale, 1999). No systematic variation in illite crystallinity or composition was revealed across the deposit.

Kaolinite group minerals occur as monomineralic aggregates filling vugs within carbonate mineral and quartz aggregates.

Limited SWIR analyses (3 samples) indicate that kaolinite is dominant, with only minor dickite identified.

Paragenetic and zoning relationships

Vuggy textures in and surrounding the mineralized zone suggest that decarbonatization and dissolution may have been initiated prior to silicification. The preservation of delicate internal and external bioclast structures in secondary quartz, however, indicates that decarbonatization and silicification of the bioclastic limestone were largely simultaneous. Drusy quartz lining vugs suggests that quartz precipitation continued after decarbonatization in the mineralized zone. The presence of carbonate minerals in vugs within the siliceous matrix and bioclast centers, in addition to the sporadic occurrence of crosscutting carbonate veinlets, indicate that carbonatization followed silicification.

The Mn carbonate minerals rhodochrosite and kutnohorite are concentrated in a proximal zone overlapping the center of the deposit, while hydrothermal calcite comprises the more distal carbonate phase. Analysis by Minera Homestake Chile of underground samples collected through the tunnel access into Jerónimo suggests an almost complete separation between Mn carbonate minerals and calcite, implying a sudden decrease in the Mn/Ca ratio away from the center of the deposit. Late carbonate minerals occur as crosscutting veins and fracture infills of calcite, generally associated with orpiment, realgar, and cinnabar.

The occurrence of illite patches and finely dispersed illite within the siliceous matrix throughout the entire deposit suggests that illite deposition occurred during silicification. However, the presence of illite in vugs in quartz and carbonate mineral aggregates indicates that its deposition continued after the bulk of the silicification. Kaolinite, which is spatially restricted to the core of the deposit proximal to the major high-angle faults, occurs in vugs within quartz and Mn carbonate aggregates. Kaolinite therefore formed after silicification and Mn carbonatization but may have overlapped temporally with the formation of illite in vugs. The predominance of kaolinite over dickite suggests formation at relatively low temperatures.

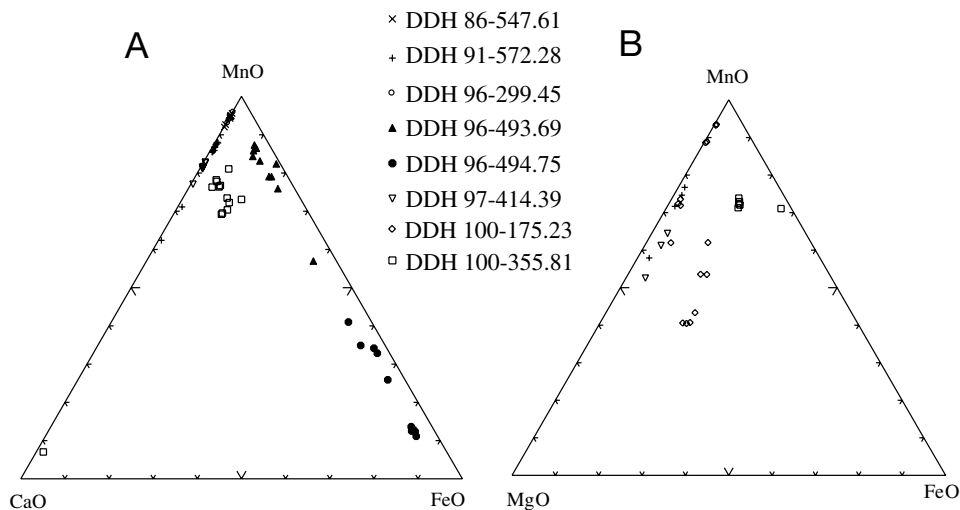


FIG. 6. Composition of (A) calcite group of carbonate minerals with <5 mol percent MgO, and (B) dolomite group minerals with 40 to 60 mol percent CaO.

Ore Mineralogy and Chemistry

Sulfide-sulfosalt mineralogy

The majority of the ore minerals in the Jerónimo deposit are restricted to small grain sizes, <1 μm to several hundred microns, necessitating the use of a scanning electron microscope (SEM) for identification and textural examination. The major sulfide and sulfosalt minerals in the Jerónimo deposit are pyrite, arsenopyrite, sphalerite, orpiment, realgar, galena, and probably several Pb sulfosalts. Minor but important sulfide phases include tellurides and Mn sulfides.

Pyrite is ubiquitous throughout the deposit and forms fine-grained, euhedral to anhedral, commonly irregular to vuggy crystals, normally ranging from 2 μm to 0.5 mm but typically ~20 μm (Fig. 7A-B). It occurs mainly as disseminated grains within quartz and carbonate aggregates and is intergrown with illite in vugs. Pyrite forms rare, diffuse, discontinuous veinlets (typically 60–100 μm across) that crosscut the silicified matrix and bands that concentrically rim silicified bioclasts. In these instances, pyrite grains are typically adjacent to or intergrown with subhedral rutile. Pyrite occurs locally in isolated framboids, typically 10 to 15 μm in diameter,

composed of aggregates of micron-sized, rounded, spherical pyrite grains or as clusters of framboids typically 80 by 60 μm . The framboidal texture may be inherited from primary or diagenetic pyrite.

Arsenopyrite occurs as subhedral to euhedral prismatic grains, typically 50 by 35 μm , disseminated in quartz and Mn carbonate aggregates. It also occurs in association with pyrite, as partial rims typically 1 μm wide in pyrite grains (Fig. 7A), as 1- to 20- μm anhedral inclusions in pyrite (Fig. 7B), and as veinlets filling fractures in pyrite.

Disseminated sphalerite grains are anhedral to subhedral and occur dominantly within Mn carbonate aggregates. Sphalerite ranges from submicron-sized equant, anhedral grains to subhedral, tabular grains, typically 80 by 35 μm . Galena is normally micron sized and anhedral, occurring within vugs in quartz and manganese carbonate. It also occurs locally as larger, typically 40- μm , subhedral, cubic inclusions in quartz aggregates.

Lead sulfosalt minerals are present mainly as tabular to acicular grains, ranging from 8 by 1 to 45 by 6 μm , in vugs within quartz. Analysis by SEM (energy dispersive mode) indicates that either twinnite ($\text{Pb}(\text{Sb}, \text{As})_2\text{S}_4$) or guettardite ($\text{Pb}_9(\text{Sb},$

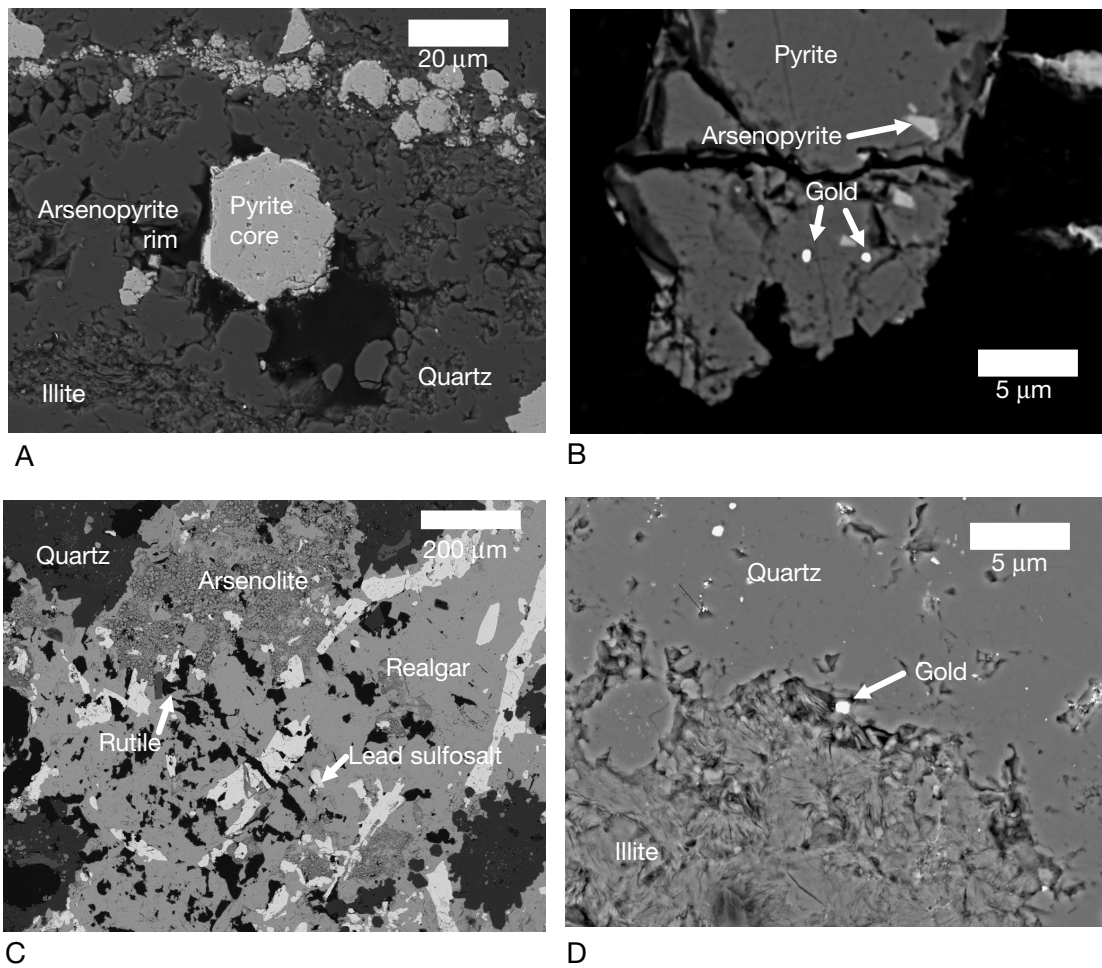


FIG. 7. Scanning electron microscope photographs, showing sulfide-sulfosalt textures and Au grains. A. Arsenopyrite rim on pyrite in vuggy quartz-illite matrix. B. Gold encapsulated in pyrite with arsenopyrite. C. Realgar-arsenolite containing Pb sulfosalts and rutile. D. Gold grain on the edge of a vug in quartz with the vug largely filled by illite.

As)₁₆S₃₃) are probably the dominant sulfosalts. The lead sulfosalts grains are locally intergrown with barite, galena, realgar, and orpiment.

Orpiment and realgar normally occur in late veinlets with calcite and minor, typically 10- μ m cinnabar grains. The As sulfide minerals also fill vugs in Mn carbonate aggregates. Locally, realgar forms large, typically 1-cm, vug-filling aggregates hosting inclusions of Pb sulfosalts, sphalerite, cinnabar, apatite, arsenolite (AsO), coloradoite (HgTe), and gold (Fig. 7C), indicating simultaneous deposition of these phases.

The deposit hosts a number of minerals that occur locally as submicron-sized grains. Typically, 600-nm grains of cassiterite are present as rounded inclusions in rhodochrosite, kutnohorite, siderite, quartz, and pyrite and locally occur in illite-filled vugs. Rare stibnite is present as anhedral, submicron-sized inclusions in rhodochrosite. Two telluride minerals are present locally, coloradoite (HgTe) and altaite (PbTe), occurring as micron-sized inclusions in quartz.

The Mn sulfides, alabandite (MnS) and hauerite (MnS₂), occur outside the ore zone in the sandy bioclastic unit E. Alabandite was also found in one sample within the ore zone where it occurs as inclusions within calcite. Alabandite and hauerite in unit E occur as veins and matrix fill in brecciated and strongly silicified-argillized wall rock associated with abundant quartz, gypsum, and calcite. Although hauerite veins crosscut alabandite veins, hauerite also occurs as inclusions in alabandite, suggesting that the minerals were more or less contemporaneous. Other minerals spatially associated with alabandite-hauerite include pyrite, Mn-rich sphalerite, galena, oldhamite (CaS), barite, apatite, monazite, rutile, and Pb-Cu sulfosalts. Electron microprobe analyses of hauerite indicate a remarkably pure composition with <0.05 wt percent substitution of As, Sn, Pb, and Cd (Gale, 1999).

Gold characteristics

Fifteen Au grains were located in six polished sections inspected by SEM. Gold occurs as anhedral, submicron- to micron-sized free grains (177 nm–1.89 μ m), in association with a variety of minerals. Gold grains most commonly occur in the linings of vugs in quartz, which may be open or filled by fine-grained illite (Fig. 7D). Gold grains are also encapsulated in the quartz matrix or are present as inclusions in grains of pyrite and arsenopyrite that are disseminated in the vuggy

quartz matrix (Fig. 7B). In one sample, Au occurs as inclusions within large (2 \times 1.5 cm) realgar aggregates and in two cases Au is spatially associated with tellurides. Analysis by SEM (energy dispersive mode) indicates that the Au hosts minor Ag but considerably less than the 30 wt percent minimum required for electrum.

Geochemistry

The average concentrations of elements in ore-grade samples from the Jerónimo intercepts logged in this study are presented in Table 1. The Jerónimo ore samples are characterized by high concentrations of As, Mn, Zn, Pb, Sb, Ag, and Hg as expected from the mineralogy discussed above. Elements that correlate well with Au include As, Hg, Te, Pb, Sb, Fe, and Mn (Gale, 1999). Similar correlations, with the addition of Ag, were reported by Simian (2000) for a larger dataset. The relationship of Mn to Au varies spatially within the deposit. At the center of it (DDH 96), the concentration of Mn correlates strongly with Au, whereas in peripheral holes Mn locally correlates with the upper Au peak but more typically forms an envelope around the ore zone.

Fluid and Metal Sources

Oxygen and carbon isotopes

The oxygen and carbon isotope compositions of ore zone rhodochrosite and kutnohorite were measured in order to constrain the character and potential source(s) of the mineralizing fluid. Calcite and dolomite from the Asientos Formation host rocks were also analyzed to evaluate their potential contribution.

Six ore zone rock samples bearing Mn carbonate minerals and four Asientos Formation limestone host-rock samples were analyzed. Samples included crushed host rocks and Mn carbonate-rich rock fragments and Mn carbonate grains that were picked out from disaggregated samples. The oxygen and carbon isotope compositions of the samples were determined at the Department of Geological Sciences Stable Isotopes Laboratory, Queens University, Canada. Details of the dissolution methods for carbonate minerals and analytical procedures are provided in Gale (1999). Isotopic compositions are reported in normal per mil deviations ($\delta^{13}\text{C}$ and $\delta^{18}\text{O}$) from standards—Cretaceous Peedee Formation belemnite (PDB)

TABLE 1. Elemental Abundance in Ore¹ from the Jerónimo Carbonate-Replacement Gold Deposit

Element	Average	Range	Element	Average	Range
Ag (ppm)	9.28	0.1–347	K (%)	0.14	0.005–0.81
Al (%)	0.41	0.06–2.29	La (ppm)	12.16	0.5–57
As (%)	0.94	0.02–42.4	Mg (%)	0.49	0.005–2.96
Ba (ppm)	25.68	0.5–159	Mn (ppm)	26956	35–257,400
Ca (%)	2.53	0.02–15	Ni (ppm)	13.11	0.5–40
Cu (ppm)	9.96	0.5–142	Pb (ppm)	2132	1–53,900
Fe (%)	4.15	0.65–10	Sb (ppm)	145.46	2–2000
Hg (ppm)	10.51	0.08–100	Zn (ppm)	5439	6–97,000

Notes: Multielement analyses performed at the Chemex Laboratory, Reno, Nevada, by ICP emission spectroscopy and cold vapor atomic absorption spectroscopy for Hg; the samples were digested using a nitric acid-aqua regia leach procedure, which may result in only partial digestion of Al and Ba and semi-quantitative analyses

¹ Ore with Au greater than or equal to 1 g/t for drill holes logged in this study (140 samples, 9 drill holes, 12 ore zone intercepts)

for carbon and Vienna standard mean ocean water (VSMOW) for oxygen (Table 2). The ore zone minerals range in $\delta^{13}\text{C}$ values from -2.84 to -1.3 per mil and in $\delta^{18}\text{O}$ values from 17.97 to 22.52 per mil, while the Asientos Formation host rocks range in $\delta^{13}\text{C}$ values from -1.83 to $+1.42$ per mil and in $\delta^{18}\text{O}$ values from 13.13 to 23.87 per mil. Only two of the host rock samples possess isotopic compositions within the field typical of marine Jurassic carbonates ($\delta^{18}\text{O} = 23\text{--}29\text{‰}$ and $\delta^{13}\text{C} = -2$ to $+3\text{‰}$) defined by Veizer and Hoefs (1976), the majority being 5 to 10 per mil lighter, probably due to reaction with an isotopically light fluid.

Since the ore zone carbonate minerals were precipitated directly from a hydrothermal fluid, the isotopic composition of these minerals can be used to constrain the isotopic composition of the fluid in equilibrium with the minerals (Ohmoto, 1986). Fluid temperature, oxygen fugacity, and pH must be known in order to calculate fluid isotopic composition from mineral isotopic data.

Fluid isotopic compositions were calculated over a range of temperatures from 200° to 350°C . This range was chosen because although not directly related to the carbonate minerals, illite intergrown with the vuggy quartz constrains fluid temperatures to between 230° and 320°C (Reyes, 1990); and reported values of fluid inclusion homogenization temperatures from Carlin-type Au deposits generally range from 175° to 300°C (Kuehn and Rose, 1992; Hofstra and Cline, 2000) and for carbonate-replacement deposits from 200° to 500°C (Haynes and Kesler, 1988; Megaw et al., 1988; Beaty et al., 1990; Titley, 1991).

The $\delta^{13}\text{C}$ of a fluid is also influenced by the types and proportions of the carbon species present. As carbon is present in carbonate minerals in the Jerónimo ore zone, the minerals were most likely in equilibrium with an oxidized C^{4+} -bearing fluid. In an oxidized fluid, pH controls whether carbon is present as CO_2 , HCO_3^- , H_2CO_3^* , or CO_3^{2-} . At temperatures of $<350^\circ\text{C}$, the dominant carbon species are H_2CO_3^* , HCO_3^- , and

CO_3^{2-} (Ohmoto and Rye, 1979). At a temperature of approximately 275°C , the intermediate value used for fluid calculations, the pH of the fluid that deposited the carbonate minerals most likely ranged from 3.5 to 7.5, with lower values more likely given the importance of illite, the local presence of aluminophosphate-sulfate minerals, and the formation of kaolinite late in the hydrothermal system. Under these conditions, the dominant carbon species in the fluid is H_2CO_3^* (Rimstidt, 1997). Although some oxygen would be derived from H_2CO_3^* , the $\delta^{18}\text{O}$ of the fluid would be dominated by H_2O . Therefore, the $\delta^{18}\text{O}$ of fluid was only calculated for equilibria between the carbonate minerals and H_2O . As limited data exist for oxygen and carbon isotope fractionations between the fluid and Mn carbonate minerals, fractionation factors for dolomite are used.

Figure 8 shows the variation in the isotopic composition of H_2O and H_2CO_3^* species of fluids in equilibrium with the ore minerals and unaltered Jurassic limestone samples. For the fluid that deposited the ore zone Mn carbonate minerals, at the intermediate temperature for 275°C , the calculated fluid $\delta^{18}\text{O}_{\text{H}_2\text{O}}$ ranges from 10.5 to 16.3 per mil, while the $\delta^{13}\text{C}_{\text{H}_2\text{CO}_3^*}$ ranges from -8.0 to -6.5 per mil. A fluid in equilibrium with the Jurassic limestone samples, at 275°C , is distinctly different with $\delta^{18}\text{O}_{\text{H}_2\text{O}}$ ranging from 16.8 to 17.5 per mil and a $\delta^{13}\text{C}_{\text{H}_2\text{CO}_3^*}$ ranging from -4.0 to -3.0 per mil.

The ore fluid $\delta^{13}\text{C}_{\text{H}_2\text{CO}_3^*}$ overlaps with the accepted range for magmatic CO_2 (Ohmoto and Rye, 1979) but could involve a mixture of components with some input from dissolved host-rock limestone and organic material (-25 to -10‰). The values of $\delta^{18}\text{O}_{\text{H}_2\text{O}}$ for the ore zone fluid at 275°C range from 10.5 to 16.3 per mil. These values are heavier than typical meteoric fluid (-10‰) but partially overlap with both the ranges for magmatic H_2O ($7\text{--}13\text{‰}$) and O derived from the dissolution of the host carbonate ($16\text{--}18\text{‰}$). The $\delta^{18}\text{O}$ values of ore zone Mn carbonate minerals, therefore, suggest that the fluid from which they were deposited included magmatic

TABLE 2. Mn Carbonate Ore Zone Asientos Formation Calcite and Dolomite Samples Analyzed for $\delta^{13}\text{C}$ and $\delta^{18}\text{O}$

Sample no.	Mineral	$\delta^{13}\text{C}$ (PDB)	$\delta^{18}\text{O}$ (VSMOW)	Description
86-547.61	Mn carbonate	-1.72	16.65	Massive, vuggy aggregates of rhomb-shaped rhodochrosite with kutnohorite at vug margins
91-562.80	Dolomite	-1.91	20.92	Vein of dolomite crosscutting fossiliferous, calcitic matrix
91-572.28a	Mn carbonate	-1.97	18.41	Massive, vuggy aggregates of rhomb-shaped rhodochrosite with kutnohorite at vug margins
91-572.28b	Mn carbonate	-2.66	17.97	As above—from different part of sample
96-299.45	Mn carbonate	-1.3	19.37	Disseminated, subhedral, rhomb-shaped rhodochrosite in quartz matrix
100-175.23	Mn carbonate	-1.91	22.52	Disseminated, subhedral rhomb-shaped kutnohorite in vugs in quartz
100-355.81	Mn carbonate	-2.84	18.45	Massive, vuggy aggregates of rhomb-shaped rhodochrosite with kutnohorite at vug margins
DDH20181-459.15	Calcite	1.42	23.87	Bioclastic limestone with sparry matrix, composed of $<90\%$ calcite
DM1-438.91	Calcite	-1.45	13.13	Carbonate veins (mainly dolomite) crosscutting matrix of carbonate grains and quartz
	Dolomite	-1.28	12.49	
DM1-438.91	Calcite	-0.88	15.23	Matrix of carbonate grains (mainly calcite) and chalcedonic quartz
	Dolomite	-1.83	12.27	
DM3-360.28a	Calcite	0.04	15.78	Calcite grains in sparry dolomite matrix
	Dolomite	-0.05	16.52	
DM3-360.28b	Calcite	0.22	15.72	Sample duplicate taken from different area of sample and crushed separately
	Dolomite	0.56	18.58	
DM3-560.00	Calcite	0.44	23.18	Bioclastic limestone with calcite spar cement

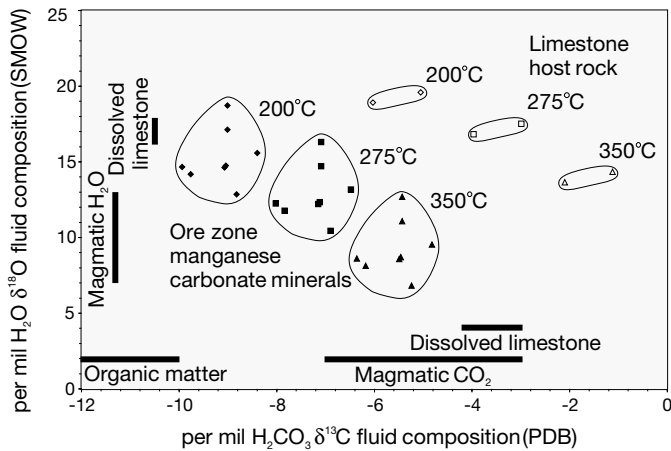


FIG. 8. Calculated O and C isotope composition of ore fluids over range of temperatures. Fractionation factors between rhodochrosite, kutnohorite, and dolomite fluid pairs are calculated using dolomite fluid equilibria of Mathews and Katz (1977), Ohmoto and Rye (1979), and O'Neil et al. (1969).

volatiles and material derived from the dissolution of the host Asientos Formation limestone. The $\delta^{18}\text{O}$ and $\delta^{13}\text{C}$ values of minerals in the pre-Jurassic basement were not analyzed in this study and a potential contribution from this source cannot be ruled out.

Lead isotopes

The Pb isotope composition of ore-related minerals has been widely used to constrain the source(s) of hydrothermal ore-forming fluids as well as the influence of the material through which the fluids were transported (summarized by Tosdal et al., 1999). Although widely applied in many ore-forming environments, relatively few studies have been undertaken on the sediment-hosted, disseminated Au deposits spatially associated with shallow-level plutonic complexes. At Jerónimo, Pb isotope compositions were determined on a suite of ore zone sulfide and sulfosalt minerals (Table 3) that appear to postdate the main phase of silicification, occurring either as veins or bands crosscutting the quartz matrix or as minerals included in vugs within it. It is difficult to relate most of these sulfide and sulfosalt minerals directly to Au, with the exception of realgar in sample DDH97-273.06d, which encapsulates Au grains, although general paragenetic relationships suggest that most of these phases are contemporaneous. In contrast, orpiment is commonly restricted to late veins with realgar, calcite, and minor cinnabar.

Additional Pb isotope data (Table 3) are reported for sulfide minerals from the nearby magmatic-hydrothermal systems at Potrerillos and El Hueso. Lead isotope data are also available for feldspar from various late Eocene to early Oligocene porphyry intrusions in the Potrerillos area, whole-rock samples of and the upper Paleozoic to Jurassic sedimentary rocks in the surrounding region (including the Asientos Formation that hosts the Jerónimo deposit), and whole rock and feldspar from the Carboniferous and Permian plutonic complexes in the region.

As is common elsewhere in the central Andes (Tosdal et al., 1999; Macfarlane et al., 1990; Tosdal and Munizaga, 2003), the potential rock sources define distinct fields in Pb isotope

covariation diagrams (Fig. 9). In general, Paleozoic to Triassic igneous and sedimentary rocks define broad fields that lie above the average crustal growth curve of Stacey and Kramers (1975) at high $^{207}\text{Pb}/^{204}\text{Pb}$ and $^{208}\text{Pb}/^{204}\text{Pb}$ values. Carboniferous plutonic rocks, which underlie the host sedimentary rock sequence at Jerónimo, form a field along the average crustal growth curve but extend to higher $^{207}\text{Pb}/^{204}\text{Pb}$ values. Jurassic to Oligocene igneous rocks in central Chile generally lie beneath the average crustal growth curve at low $^{207}\text{Pb}/^{204}\text{Pb}$ values (Tosdal and Munizaga, 2003; R.M. Tosdal unpub. data, 2003). Jurassic sedimentary rocks, which also host the Jerónimo deposit, have the most distinctive Pb isotope field, plotting at lower $^{207}\text{Pb}/^{204}\text{Pb}$ and $^{208}\text{Pb}/^{204}\text{Pb}$ values for a given $^{206}\text{Pb}/^{204}\text{Pb}$ than any of the other potential sources of Pb. The low $^{208}\text{Pb}/^{204}\text{Pb}$ and elevated $^{206}\text{Pb}/^{204}\text{Pb}$ values, and by implication low Th/U, are distinctive of carbonate rocks, which dominate the Jurassic sedimentary sequence. These rocks also define the high $^{206}\text{Pb}/^{204}\text{Pb}$ part of the Jurassic field, whereas the clastic-rich rocks form the low $^{206}\text{Pb}/^{204}\text{Pb}$ field (see Table 3). The distinct fields for rocks of various ages and for different compositions of Jurassic sedimentary rocks in the immediate region of the Jerónimo deposits provide a critical constraint on potential sources of Pb, and by inference other metals, in the sediment-hosted deposit.

Sulfide and sulfosalt minerals from Jerónimo have two distinct Pb isotope characteristics. Most of the minerals, with the exception of late orpiment, are characterized by limited values of $^{206}\text{Pb}/^{204}\text{Pb}$ (18.56–18.61), but a range of $^{207}\text{Pb}/^{204}\text{Pb}$ (15.57–15.66) and $^{208}\text{Pb}/^{204}\text{Pb}$ (38.54–38.64) that define a steep trend in the variation diagram (Fig. 9). The steep trend extends parallel to and beyond the array defined by sulfide minerals from porphyry Cu-Mo-(Au) mineralization at Potrerillos and Au mineralization at El Hueso. The high $^{207}\text{Pb}/^{204}\text{Pb}$ and $^{208}\text{Pb}/^{204}\text{Pb}$ values for the Jerónimo, as well as the Potrerillos porphyry Cu-Mo-(Au) deposit, overlap in the field for late Paleozoic sedimentary rocks although the Carboniferous plutonic rocks in the basement to the Potrerillos area cannot be excluded as a source. Steep trends in $^{207}\text{Pb}/^{204}\text{Pb}$ values could be attributed to thermal fractionation during analysis, but steep trends in these data are also typical of Tertiary ore deposits in the Andes that are located where high $^{207}\text{Pb}/^{204}\text{Pb}$ Paleozoic rocks are common (Macfarlane et al., 1990; Tosdal et al., 1995; summarized by Tosdal et al., 1999). Furthermore, the effect of thermal fractionation is rarely seen in the $^{208}\text{Pb}/^{204}\text{Pb}$ values, and the steep trend in that diagram is considered to reflect real Pb isotope variations.

In contrast, orpiment defines a separate trend, with the Pb isotope compositions departing from the main cluster toward higher $^{206}\text{Pb}/^{204}\text{Pb}$ (18.7 and 19.2) but with little variation in either $^{207}\text{Pb}/^{204}\text{Pb}$ or $^{208}\text{Pb}/^{204}\text{Pb}$ values. These values indicate that a component of Pb in these minerals was characterized by low Th/U. Lead isotope compositions for orpiment plot between the low $^{207}\text{Pb}/^{204}\text{Pb}$ and $^{208}\text{Pb}/^{204}\text{Pb}$ part of the Eocene porphyry and sulfide field and the Jurassic sedimentary rock field, typical of the Asientos and Pedernales Formations (Table 3).

The Pb isotope compositions of the sulfide and sulfosalt minerals reflect the mixing of Pb from the Eocene to

TABLE 3. Pb Isotope Compositions of Ore Minerals, Igneous Rocks, and Sedimentary Rocks from the Vicinity of the Jerónimo Sediment-Hosted Au Deposit, Central Chile

Sample no.	Minerals	$^{206}\text{Pb}/^{204}\text{Pb}$	$^{207}\text{Pb}/^{204}\text{Pb}$	$^{208}\text{Pb}/^{204}\text{Pb}$	Sample no.	Minerals	$^{206}\text{Pb}/^{204}\text{Pb}$	$^{207}\text{Pb}/^{204}\text{Pb}$	$^{208}\text{Pb}/^{204}\text{Pb}$
Jerónimo ore minerals					Eocene				
DDH86-546.58	Orpiment	18.695	15.607	38.622	IT-13	Cobre porphyry-plag.	18.551	15.603	38.506
DDH93-527.33	Orpiment	19.119	15.656	38.687	EH-33	El Hueso porphyry-plag.	18.508	15.582	38.415
DDH93-533.07b	Galena	18.644	15.653	38.632	EH-25	Cobre porphyry-plag.	18.530	15.591	38.456
DDH97-273.06a	Sphalerite	18.582	15.623	38.566	EH-39	Bochinche porphyry-plag.	18.537	15.594	38.470
DDH97-273.06b	Sphalerite	18.564	15.592	38.589	Bochinche	Bochinche	18.547	15.617	38.532
DDH97-273.06c	Pb sulfosalt	18.579	15.618	38.554	EH-41	Norte porphyry-plag.	18.534	15.592	38.459
DDH97-273.06d	Realgar	18.573	15.617	38.540	Sedimentary rocks				
DDH97-277.17	Galena	18.614	15.662	38.638	Carboniferous				
DDH97-282.89	Galena	18.589	15.635	38.606	RCB-52	Sandy siltstone	18.687	15.647	39.060
DDH97-287.25	Sphalerite	18.567	15.611	38.536	RCB-53	Sandy siltstone	18.921	15.715	39.155
Cobre porphyry					RCB-54	Sandy siltstone	19.568	15.732	39.785
PO-1	Chalcopyrite	18.561	15.606	38.516	RCB-56	Sandy siltstone	19.340	15.709	39.319
IT-13	Chalcopyrite-pyrite	18.527	15.598	38.490	MECA-21	Siliceous siltstone	18.469	15.661	38.649
EH93-35	Galena	18.606	16.608	38.540	MECA-22	Quartz arenite	18.450	15.645	38.512
EH93-35	Tennantite	18.588	15.618	38.576	Permo-Triassic				
EH93-35	Pyrite	18.643	15.640	38.538	MECA-25A	Quartz sandstone	18.650	15.668	38.756
El Hueso					MECA-25B	Shale	18.800	15.655	38.870
PB-1a	Pyrite	18.628	15.637	38.653	MECA-25C	Volcaniclastic sandstone	18.871	15.652	39.003
PB-1b	Pyrite	18.602	15.604	38.543	Triassic				
PB-2a	Pyrite + quartz/ carbonate	18.602	15.606	38.552	MECA-1A	Reddish shale	18.858	15.688	39.019
PB-2b	Pyrite	18.603	15.618	38.591	MECA-1B	Reddish sandstone	18.813	15.648	38.917
PB-2b	Pyrite + quartz/ carbonate	18.603	15.608	38.559	Jurassic				
Igneous rocks					DM1-438.91	Calcite-dolomite	19.245	15.691	38.833
Carboniferous					DM3-360.40	Calcite in sparry dolomite	18.941	15.541	38.237
Sierra Castilla batholith					DM3-560.00a	Bioclastic limestone	18.887	15.632	38.791
IT-14 Kf	Diorite	18.435	15.610	38.306	DM3-560.00b	Bioclastic limestone	19.005	15.735	39.071
IT-15 Kf	Granodiorite	18.475	15.626	38.397	DDH20181- 459.15	Bioclastic limestone	22.306	15.775	40.573
IT-16 Kf	Monzogranite	18.729	15.692	38.687	DDH20181- 459.15	Bioclastic limestone	22.163	15.729	40.395
Permian					DDH91-562.80	Dolomite in veins	19.173	15.754	38.975
Pedernales batholith					Aguas Heladas Formation				
RCB-252	Diorite	18.902	15.655	39.138	MECA-2	Reddish-brown sandstone	18.822	15.630	38.660
MECA-40 Kf	Diorite	18.582	15.651	38.666	MECA-9A	Sandstone	18.897	15.644	38.780
MECA-6	Diorite enclave	19.338	15.671	39.415	MECA-9B	Siltstone	18.825	15.637	38.713
MECA-5	Granodiorite	19.346	15.674	39.608	MECA-11	Calcareous sandstone	19.534	15.691	39.313
MECA-5 Kf	Granodiorite	19.056	15.655	39.083	MECA-14	Calcareous sandstone	18.874	15.632	38.636
MECA-17	Granodiorite	19.345	15.675	39.546	MECA-16	Fossiliferous limestone	19.559	15.672	38.802
RCB-253	Porphyritic granite	19.674	15.698	39.677	MECA-18	Calcareous sandstone	19.651	15.689	39.096
MECA 41 Kf	Porphyritic granite	18.744	15.666	38.708	MECA-19	Fossiliferous limestone	18.994	15.646	38.686
RCB-251	Aplite	18.876	15.661	38.849	MECA-23B	Siltstone	18.770	15.641	38.754
MECA-7	Aplite	19.947	15.724	39.915	Jurassic				
Permo-Triassic					MECA-12				
MECA-24A	Rhyolite	18.790	15.642	38.828	MECA-13	Andesite	18.619	15.607	38.499
MECA-24B	Rhyolite	19.110	15.661	39.224	MECA-13				
RCB-218	Rhyolite	18.891	15.662	38.955	MECA-13				
RCB-214	Syenogranite	18.809	15.642	38.928	MECA-13				
MECA-31 Kf	Syenogranite	18.556	15.611	38.574	MECA-13				
MECA-30 Kf	Rhyolite	18.814	15.667	38.894	MECA-13				
MECA-32 Kf	Syenogranite	18.581	15.621	38.588	MECA-13				

Notes: Samples from Jerónimo and the El Asiento Formation were analyzed at the University of British Columbia; details of the analytical methods are reported in Gale (1999); all other samples were analyzed at the U.S. Geological Survey in Menlo Park using analytical methods described by Bouse et al. (1999); lead isotope compositions for the Potrerillos porphyry Cu-Mo deposit, with the exception of IT-13, were previously reported in Marsh (1997); analytical uncertainties for all analyses are better than 0.1 percent (2σ)

Abbreviations: Kf = K-feldspar; plag. = plagioclase; all other samples are from whole-rock samples and represent present-day values

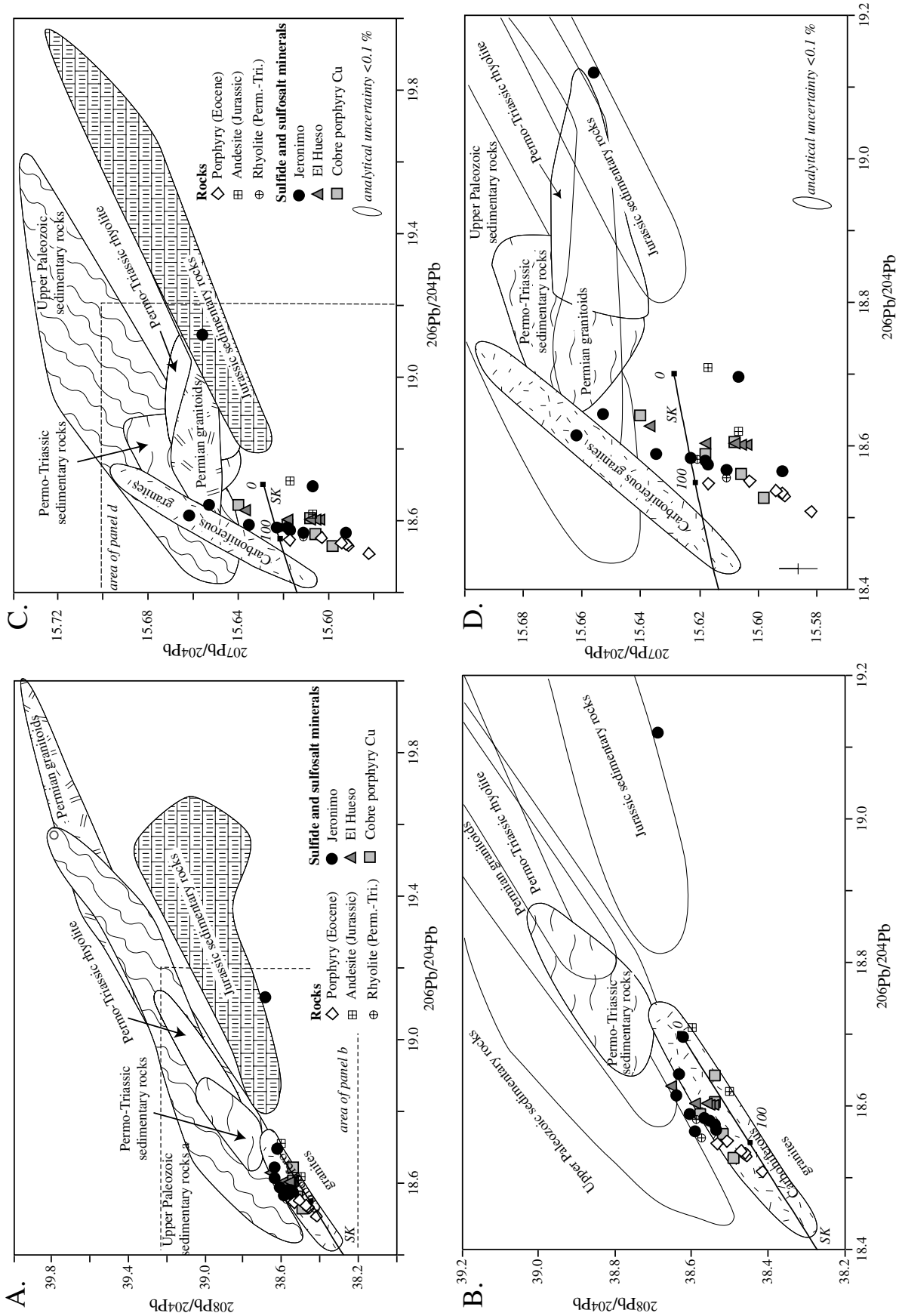


FIG. 9. A and B. $^{208}\text{Pb}/^{204}\text{Pb}$ vs. $^{206}\text{Pb}/^{204}\text{Pb}$, and C and D. $^{207}\text{Pb}/^{204}\text{Pb}$ vs. $^{206}\text{Pb}/^{204}\text{Pb}$ isotope evolution diagrams, showing potential Pb sources in the Jerónimo deposit. Fields are shown for sedimentary and igneous rocks as well as the sulfide Pb isotope compositions from nearby deposits (Table 3). SK = average crustal growth curve of Stacey and Kramers (1975). Analytical uncertainties are <0.1 percent and are slightly larger than the symbols in panels A and B.

Oligocene porphyries with Pb from one of two other distinct sources. One source is characterized by high $^{207}\text{Pb}/^{204}\text{Pb}$ and $^{208}\text{Pb}/^{204}\text{Pb}$, which characterizes the late Paleozoic sedimentary rocks or the Carboniferous plutonic rocks, both of which lie in the subsurface beneath Jerónimo. This Pb was likely scavenged or contributed to the hydrothermal ore fluid during its passage from the porphyry to the site of ore deposition. Addition of external Pb to a magmatic-hydrothermal fluid is noted in several porphyry Cu deposits (Bouse et al., 1999; Tosdal et al., 1999) and is thus not unexpected in a deposit distal from the magmatic source. In contrast, the Pb in the late orpiment requires a different source, which most likely is the carbonate-rich host rocks. Lead from this source must have been added by an influx of hydrothermal or meteoric fluid during the late-stage collapse of the system. Tosdal et al. (2003) noted a late addition of locally derived Pb from host calcareous sequences in the Carlin-type Au deposits in Nevada.

Discussion

Controls on alteration and mineralization

Jerónimo is a mantolike, disseminated Au deposit, hosted by Jurassic marine limestone. Alteration and mineralization are dominantly hosted in coarse-grained bioclastic horizons (unit C) with only rare sand grains and little detrital or diagenetic clay. In contrast, fine-grained silty and sandy limestone, located above and below the ore zone, and also interfingering with it, host only minor mineralization. The bioclastic limestone horizons are favorable ore hosts because of their relatively high porosity and permeability, resulting from their (1) large grain size, (2) irregular grain shape, (3) lack of clay particles clogging pore space, (4) high intraparticle porosity, and (5) high fracture-related secondary porosity. Probable conduits for mineralizing fluid include the steep normal faults that transect the orebody, are premineral in age, and host minor mineralization.

The earliest alteration events are decarbonatization and silicification. Decarbonatization may have preceded silicification, resulting in the local development of vuggy textures. Subsequent silicification pervasively replaced limestone while preserving delicate bioclast structures. Disseminated pyrite, arsenopyrite, sphalerite, rutile, apatite, barite, and micron-sized monazite are partially encapsulated by the quartz matrix. Decarbonatization and simultaneous silicification of the host limestone most likely occurred due to cooling of the hydrothermal fluid. At temperatures below 300°C and at a constant value of f_{CO_2} , calcite solubility increases and quartz solubility decreases as temperature decreases (Fournier, 1985a). If the fluid was relatively acidic, as suggested below, neutralization during reaction with wall-rock carbonates may also have promoted silicification. Although the salinity of the ore fluid is unconstrained, elevated salinities are typical of fluids in carbonate-replacement deposits and will likely aid dissolution due to enhanced carbonate solubilities.

Carbonatization within the Jerónimo deposit is marked by the precipitation of Mn and Ca carbonate minerals. Aggregates of Mn carbonate minerals, rhodochrosite and kutnohorite, are dominant in an elliptical zone in the center of the deposit. Mn carbonate minerals encapsulate pyrite, sphalerite,

rutile, rhodonite, barite, and monazite, and vugs in Mn carbonate aggregates are filled mainly by orpiment, realgar, and kaolinite. Hydrothermal calcite with some dolomite (locally manganoan) occurs in the outer part of the deposit and in late fractures associated with calcite, orpiment, realgar, and minor cinnabar.

The precipitation of calcite in hydrothermal systems is largely controlled by f_{CO_2} , which varies mainly by the processes of boiling, as mentioned above, and fluid mixing (Simmons and Christenson, 1994). Postsilicification of carbonate may therefore reflect boiling and loss of CO_2 (Fournier, 1985b), possibly as a result of decrease in fluid pressure when ascending fluid encounters open spaces, such as vugs and fractures (Gieré, 1996). Although carbonate minerals in Jerónimo occur in vugs, the lack of platy carbonate texture (Simmons and Christenson, 1994) suggests that boiling was not a major process and mixing may have been more important. The compositional zonation of the Jerónimo carbonate minerals reflects the Mn/Ca ratio in the hydrothermal fluid. This ratio must have decreased as the fluid spread toward the margins of the deposit, possibly due to interaction with the host limestone or external fluid.

The Jerónimo clay mineral assemblage consists of illite and kaolinite. Illite is present in minor abundance throughout the ore zone in the vuggy quartz matrix and as finely disseminated particles and vug-filling aggregates that locally host Au grains. Illite crystallinity does not vary significantly throughout the deposit. Kaolinite occurs in vugs in a northwest-trending zone that overlaps the fault system in the center of the deposit. The presence of illite and kaolinite within the deposit indicates that Al and K were transported at least locally by the hydrothermal fluid and were possibly acquired from the alteration of detrital feldspar in units below the ore-hosting horizon. In active geothermal systems in the Philippines (Reyes, 1990), illite deposition occurs from fluid of near-neutral pH over the temperature range of 230° to 320°C, the conditions likely for the main stages of alteration in the Jerónimo deposit. In contrast, kaolinite in the Philippine geothermal systems is deposited from acidic fluid with temperatures ranging from ambient to 120°C. It is possible, therefore, that kaolinite was deposited from cooler, more acidic fluids—late upwelling hydrothermal fluids or descending acid condensate—or supergene fluid unrelated to ore formation.

There is, however, independent evidence for relatively low pH fluid since the presence of monazite and REE-bearing calcite in Jerónimo ore implies transport of REE, a process which requires acidic conditions at the temperatures suggested for Jerónimo (Gieré, 1996). Rare earth elements are often transported with elements such as Ti, which may account for the abundance of rutile in the deposit (Gieré, 1996). Further support for acidic fluid is recorded by the presence of alumino-phosphate-sulfate minerals. If correct, the primary ore fluid may have had a relatively low pH, possibly approaching the fluid composition in high-sulfidation systems that commonly contain a similar suite of trace minerals (e.g., Cooke and Simmons, 2000). Wall-rock reaction and buffering at Jerónimo would have inhibited formation of widespread advanced argillic alteration until late in the life of the system when the wall-rock buffering capacity was reduced and kaolinite was precipitated.

Major ($\geq 1\%$) minerals in the Jerónimo ore suite consist of pyrite, arsenopyrite, sphalerite, galena, Pb sulfosalt(s), realgar, and orpiment. Typically, arsenopyrite and pyrite, often in association with rutile, are disseminated within the quartz matrix. Realgar and orpiment are present mainly in late fracture and veinlets, normally with calcite and rare grains of cinnabar. Minor minerals include cassiterite, coloradoite, altaite, stibnite, and native silver. Gold occurs in native form generally as submicron-sized anhedral grains present as inclusions in pyrite and arsenopyrite or at vug margins in the quartz matrix. There are no direct constraints on the processes leading to Au deposition, but mineralogic indications of fluid mixing and possible boiling are the most likely influences on Au solubility and deposition (Seward, 1991).

Stable isotope data are consistent with a significant magmatic contribution to the ore fluid with possible contributions from host-rock limestone-carbonate or organic material. Mixing of two separate fluid sources is possible but cannot be documented directly. Lead isotope data, however, clearly reflect multiple sources including Tertiary intrusions, Paleozoic basement, and local host rocks. The Pb isotope composition of late orpiment suggests an increasing contribution of Pb from the host rocks during the late stages of mineralization.

Comparison to Carlin-type and carbonate-replacement deposits

The Jerónimo deposit can be compared to other types of sediment-hosted Au deposit, particularly the end-member Carlin-type and carbonate-replacement types. The characteristics of Carlin-type deposits have been described by many authors as summarized by Hofstra and Cline (2000). Ore deposition in this type of deposit is strongly influenced by lithology and structure. Preferential ore-hosting horizons are calcareous sandstone and siltstone, and mineralization typically fans out where steep faults intersect favorable horizons. The dominant sulfide mineral assemblage in Carlin-type deposits includes arsenian pyrite, arsenopyrite, realgar, and orpiment, and the deposits are characterized by the As-Sb-Hg-Tl association. Alteration styles in Carlin-type systems consist mainly of decalcification, silicification, and argillization, although the deposition of Ca carbonate minerals occurs in some cases, particularly on the periphery of systems. Gold occurs as thin films coating arsenian pyrite, submicron-sized inclusions of native Au in arsenian pyrite, and as structurally bound atoms of Au in arsenian pyrite (Simon et al., 1999; Hofstra and Cline, 2000). Bands of arsenian pyrite enriched in Au may also contain elevated Te, Cu, and other elements more characteristic of carbonate-replacement deposits (Henkelman et al., 2003). Although intrusions are almost always present in proximity to Carlin-type deposits, the nature of their involvement in mineralization is uncertain.

Carbonate-replacement deposits are part of a family of deposits zoned around magmatic-hydrothermal, intrusion-centered systems that include porphyry, skarn, and vein deposits (Sillitoe, 1991a). Carbonate-replacement deposits occur as replacement-style mineralization in limestone and dolostone. They are structurally and lithologically controlled, preferring permeable limestone beds, and normally occur in manto-, lens- and chimney-shaped bodies. Although typically mined for base metals, some carbonate-replacement deposits are Au

rich and possess only minor base metal enrichment (e.g., Star Pointer, Nevada; Albino, 1995). Megaw (1998) notes that silicification and jasperoid development is most common in the peripheral parts of carbonate-replacement deposit systems and that the jasperoids are locally Au bearing. Similarly, Sillitoe and Bonham (1990) proposed that Au-rich carbonate-replacement deposits form the most distal member of the sequence of intrusion-related deposits in zoned intrusion-centered camps. The dominant sulfide mineral assemblage in Au-rich carbonate-replacement deposits consist of pyrite, arsenopyrite, sphalerite, galena, chalcopyrite, marcasite, and pyrrhotite, and their geochemical signature, which is more variable than in Carlin-type deposits, consists of As-Sb-Pb-Zn \pm Ag, Mn, Tl, Te, Cu, Hg, Bi, and Sn. Like Carlin-type deposits, alteration types in Au-rich carbonate-replacement deposits consist of decarbonatization, silicification, argillization, and carbonatization. In contrast to Carlin-type deposits, igneous intrusions are known to be a major source of heat, fluid, and probably metals (e.g., Beatty et al., 1990). Gold occurs as discrete particles, normally ranging from 1 to 100 μm , which are either encapsulated in gangue and sulfide minerals or occur at mineral edges (e.g., Purísima Concepción, Peru; Alvarez and Noble, 1988). Some Au-rich carbonate-replacement deposits are enriched in Mn (e.g. Purísima Concepción; Alvarez and Noble, 1988; Cove, Nevada; Emmons and Coyle, 1988; Star Pointer, Nevada; Albino, 1995).

The Jerónimo deposit clearly shows many features characteristic of distal carbonate-replacement deposits. In particular, the importance of carbonate and distinctive minor alteration minerals (monazite, rutile, apatite, and aluminophosphate-sulfate minerals), the sulfide-sulfosalt mineralogy, significant Mn, and free Au are similar to other Au-rich carbonate-replacement deposits. Furthermore, isotopic data support a role for magmatic fluid, probably derived from Eocene to Oligocene porphyry intrusions in the area. As mentioned previously, direct isotopic evidence for magmatic fluid in Carlin-type deposits is rare.

The geochemical characteristics of the Jerónimo deposit can be compared to Carlin-type deposits using the data of Radtke (1985) and Hofstra (1994) for the Carlin and Jerritt Canyon deposits in Nevada, respectively. The concentration of Mn and Pb is >100 times greater in Jerónimo than at Carlin, and neither is significantly enriched relative to unaltered rocks at Jerritt Canyon. The concentration of Zn is >25 times greater, and As and Ag are more than an order of magnitude greater in Jerónimo relative to the Carlin-type deposits. Concentrations of Hg, Sb, and Cu are similar in both deposits, whereas Ba is more than an order of magnitude greater at Carlin than in Jerónimo. Although absolute concentrations vary among carbonate-replacement deposits, the typical metal suite is similar to that found at Jerónimo (e.g., Megaw, 1998).

Metallogenic relationships in the Potrerillos district

In addition to Jerónimo, the Potrerillos district hosts two other significant mineral deposits, the Potrerillos porphyry Cu-Mo-(Au) deposit and the carbonate- and volcanic-hosted disseminated Au-Ag deposit at El Hueso. The Potrerillos deposit, hosted in the Cobre porphyry, is located approximately 4.3 km west-northwest of Jerónimo. The Cobre porphyry was emplaced into the Montandon, Asientos, and Pedernales

Formations and produced a skarn zone extending up to 1.5 km from the porphyry contact. The Potrerillos deposit is truncated at a depth of about 400 m by the major west-dipping Potrerillos Mine fault (Tomlinson, 1994).

El Hueso is located approximately 1.5 km to the west of Jerónimo. Mineralization at El Hueso is of replacement style and is concentrated in steep, east trending faults and adjacent bioclastic limestone of the upper Asientos Formation and tuff of the Tertiary Hornitos Formation. El Hueso is also truncated by the Potrerillos Mine fault. Based on radiometric dating, Marsh (1997) interpreted the age of mineralization to be 35.6 to 35.9 Ma for Potrerillos and 40.2 to 40.8 Ma for El Hueso. Alunite from El Hueso (36.23 ± 0.07 Ma; Marsh, 1997) may represent remnants of a lithocap. Attempts during this study to define the age of mineralization at Jerónimo using U-Pb dating of rutile failed due to the limited concentration and fine grain size of rutile, and therefore, the age of Jerónimo and the potential temporal relationship to Potrerillos and El Hueso remain uncertain.

A potential genetic link between the Potrerillos and Jerónimo deposits seems possible given the size of the Potrerillos porphyry system, and the presence of synmineral, west-dipping thrust faults that project updip toward Jerónimo. Hydrothermal fluid originating from the Potrerillos porphyry deposit could have ascended along conduits, such as the west-dipping thrust faults, steep east trending faults, or the relatively porous and permeable, gently west dipping stratigraphic units (e.g., unit C). To test these possibilities, six drill intercepts of unit C extending west of Jerónimo over a distance of 1.7 km from the western limit of the deposit toward Potrerillos were logged and sampled (Fig. 10). The drill holes intersect a bedding-concordant, 2- to 18-m-thick zone of brecciation west of hole DDH 20181, lying either within or immediately below unit C. This breccia zone consists of rubbly, strongly decalcified and weakly silicified fragments of limestone with as much as 7 vol percent pyrite. Gold grades are consistently higher in the breccia than in the more competent parts of unit C

(<0.01–0.72 g/t Au). In the most distal occurrence of unit C observed in this study, the bioclastic limestone consists of a calcite matrix with illite- or kaolinite-filled vugs. Disseminated pyrite grains, locally hosting thin growth layers of arsenian pyrite, and minor disseminated rutile and sphalerite are present. Alteration and mineralization indicate that fluid flowed along unit C and the underlying breccia.

Calcite in the most westerly (DM3) and easterly (DDH 20181) drill holes from the cross section were analyzed for O, C, and Pb isotope composition (Table 3). In both cases, the calcite has O and C isotope values typical of Jurassic carbonate rocks (Veizer and Hoefs, 1976), but the Pb isotope composition of the easterly hole, adjacent to the western margin of Jerónimo, is enriched in radiogenic Pb, possibly due to an increased feldspar component in the rock. In contrast to the presence of alteration and minor mineralization, the isotopic data do not indicate significant fluid flow or an indication of flow direction along the west-dipping thrust fault or subparallel stratigraphy. While some fluid flow occurred through unit C and the associated breccia, the dominant fluid flow was likely upward through the Mapuche and Polvorines fault systems with outflow into unit C at Jerónimo and continued flow away from Jerónimo in unit C and the related footwall breccia. There is no direct evidence to support updip flow through the gently west dipping unit C, breccias, and thrusts faults from the Potrerillos porphyry Cu deposit toward Jerónimo.

Genetic model for Jerónimo

The mineralogic and geochemical composition of Jerónimo suggests a carbonate-replacement deposit affiliation and therefore a genetic model related to a magmatic-hydrothermal system. An important magmatic contribution to the ore fluid and the source of Pb is supported by stable and radiogenic isotopic data, although lesser contributions from other sources are possible. A similar magmatic-dominant source for Au is reasonable given the positive correlation of Au with Pb and Sb in the geochemical data and the occurrence of an Au

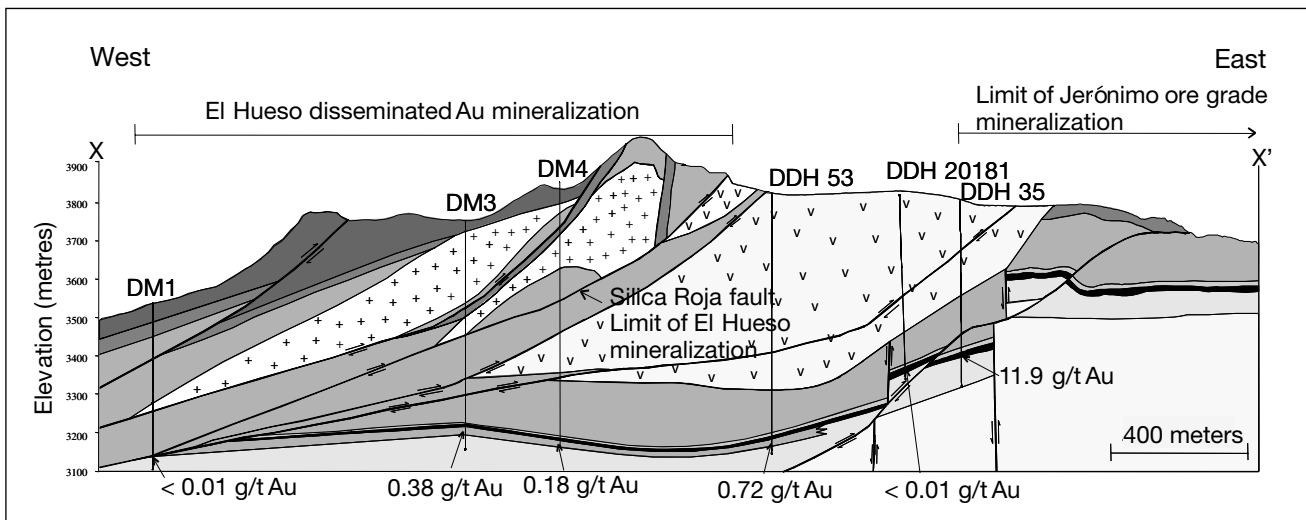


FIG. 10. Interpreted long section through the El Hueso-Jerónimo area, showing major thrust and normal faults, Au grades in drill intersections through unit C, and the footwall breccia. Several of these holes were sampled for O, C, and Pb isotopes—see text. Legend as in Figure 4.

grain in main-stage realgar that was also analyzed for its common Pb composition. Although a magmatic-hydrothermal model is preferred, the causative intrusion is not well constrained.

A second critical unknown is the precise age of mineralization at Jerónimo. Mineralizing fluid appears to have used sub-vertical faults and fractures that most likely formed during the waning stages of Eocene to Oligocene deformation (Caddey, 1999). The other major deposits in the Potrerillos district, the Potrerillos porphyry Cu-Mo-(Au) and El Hueso disseminated Au deposits, also formed during the late Eocene to early Oligocene and both show a temporal relationship to deformation in the region. Dating by Marsh (1997) demonstrated that intrusive ages in the Potrerillos district span a range from 40.4 to 32.6 Ma, with the age of El Hueso mineralization being placed at the older end of this range (~40 Ma) and the Potrerillos porphyry mineralization and an associated lithocap forming approximately 4 m.y. later (~36 Ma). Jerónimo may be temporally and genetically related to either of these events or another unknown Eocene to Oligocene magmatic-hydrothermal system.

The interpreted genetic model for Jerónimo is shown in Figure 11 with a hypothetical intrusion at depth and related fluid-flow paths. The depositional part of this model is reasonably constrained. Magmatic-dominant fluid ascended through the Mapuche and Polvorines fault systems and spread into unit C. Although paragenetically unconstrained, the presence of minor skarn alteration in the footwall of the ore zone (Fig. 4) may reflect a heat and fluid source below the deposit. At the site of deposition, a combination of wall-rock reaction and cooling of the hydrothermal fluid most likely resulted in the dissolution of the host limestone and simultaneous deposition of quartz, accompanied by the precipitation of pyrite, arsenopyrite, sphalerite, rutile, apatite, barite, monazite, and some illite. The presence of Au as inclusions in pyrite, arsenopyrite, and quartz confirms that some Au deposition occurred at this time. The deposition of monazite and rutile during silicification implies that the fluid was moderately acidic, although the precise pH is unconstrained. Neutralization of the acidic fluid may have enhanced quartz deposition. Local bulk decarbonatization and dissolution of the limestone occurred prior to silicification, creating significant open space.

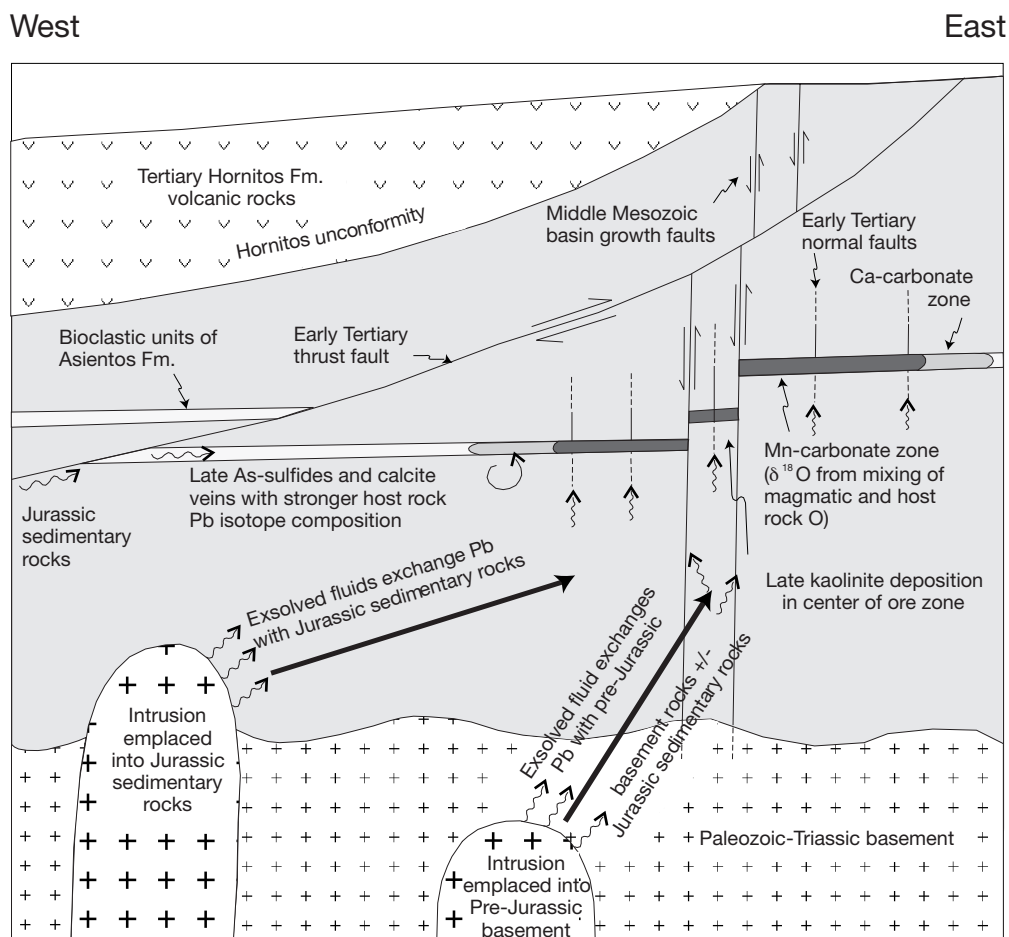


FIG. 11. Schematic model for the Jerónimo system, showing a hypothetical intrusion at depth; potential paths of fluid-flow paths (arrows with curved tails) including: (1) Mesozoic steep normal faults; (2) the early Tertiary thrust fault combined with a medium for the lateral transport of the fluid to the site of ore deposition, such as the bioclastic limestone; (3) the early Tertiary normal faults; a concentric pattern of zonation, focused on the center of the deposit, based on carbonate mineral composition; late arsenic sulfides and calcite veins were deposited from fluids that had equilibrated with the Asientos Formation host rocks; and (4) late kaolinite deposition in the center of the orebody.

Subsequently, carbonate minerals were deposited from fluid including components most likely derived from magmatic volatiles and dissolved Asientos Formation limestone. The carbonate minerals were deposited in response to a decrease in f_{CO_2} , which most likely occurred by fluid mixing. The fluid Mn/Ca ratio decreased as the fluid spread away from the center of the ore zone, possibly due to increasing interaction with external fluid and the limestone host. Pyrite, sphalerite, rutile, rhodonite, and barite were precipitated during carbonate deposition.

Following carbonatization, the deposition of illite with pyrite and apatite continued. Late alteration involved the deposition of kaolinite, with minor alumino-phosphate-sulfate minerals, in the center of the deposit, from acidic fluids with the lack of significant dickite, suggesting relatively low temperatures ($\sim 120^\circ\text{C}$). This fluid might have maintained a low pH due to a lack of remnant buffering capacity in the host rock. Alternative origins for kaolinite involving descending acid condensates related to lithocap development in the region or descending oxidized supergene fluid cannot be ruled out. There is, however, no direct evidence for descending fluid and the presence of illite-kaolinite at depth in unit C west of Jerónimo suggests that the former explanation for kaolinite is more likely.

Crosscutting calcite-orpiment-realgar veins represent the final mineralizing event. Isotopic data indicate an increased component of wall-rock Pb in these veins, possibly reflecting ingress of meteoric water. The timing of these veins relative to kaolinite formation is unknown.

Conclusions

The key features of the Jerónimo sediment-hosted disseminated Au deposit include the following:

1. Jerónimo is an Au-rich carbonate-hosted deposit carbonate-replacement deposit that formed on the eastern side of the Potrerillos district. The precise age of mineralization at Jerónimo has not been defined, but it is interpreted to be late Eocene to early Oligocene, similar in age to the Potrerillos porphyry Cu-Mo-(Au) and El Hueso Au deposits.

2. Jerónimo is both lithologically and structurally controlled. Ore is hosted in bioclastic limestone horizons, due to their enhanced primary and secondary porosity and permeability. Jerónimo mineralization is also present in steep normal faults of presumed Tertiary age.

3. Alteration types recorded in the Jerónimo ore include decarbonatization, silicification, carbonatization, and argillization. Jerónimo hosts Mn carbonate mineralization in a zone overlapping the center of the deposit. The Jerónimo clay mineral assemblage consists of illite and kaolinite. Other alteration minerals that are characteristic of Jerónimo ore are rutile, apatite, monazite, and barite.

4. The Jerónimo sulfide and sulfosalt mineral suite includes pyrite, arsenopyrite, sphalerite, galena, Pb sulfosalts, orpiment, and realgar. Coloradoite, altaite, cassiterite, and stibnite occur as occasional micron-sized grains. High concentrations of As, Mn, Zn, Pb, Sb, Ag, and Hg characterize the Jerónimo deposit. Gold is present as generally submicron-sized grains of native Au encapsulated within pyrite, arsenopyrite, realgar, and quartz or in vugs in the quartz-rich matrix of the altered limestone host.

5. The Jerónimo ore-forming fluid and contained metals were derived dominantly from a magmatic source but also incorporated material from the Jurassic sedimentary host rocks and/or the dominantly granitic pre-Jurassic basement.

Acknowledgments

The authors wish to thank Barrick Gold Corporation for permission to publish this paper. Field and analytical support for Vanessa Gale was provided by Minera Homestake (now Barrick Gold Corporation) and graduate student support was provided by the Natural Science and Engineering Council of Canada. The manuscript was improved significantly by the reviews of Peter Megaw and Tommy Thompson. This paper is MDRU contribution P-172.

REFERENCES

- Albino, G.V., 1995, Porphyry copper deposits of the Great Basin-Nevada, Utah and adjacent California: Arizona Geological Society Digest 20, p. 267–296.
- Alvarez, A.A., and Noble, D.C., 1988, Sedimentary rock-hosted disseminated precious metal mineralization at Purísima Concepción, Yauricocha district, central Peru: Economic Geology, v. 83, p. 1368–1378.
- Beatty, D.W., Landis, G.P., and Thompson, T.B., 1990, Carbonate-hosted sulfide deposits of the central Colorado mineral belt: Introduction, general discussion, and summary: Economic Geology Monograph 7, p. 1–18.
- Bouse, R.M., Ruiz, J., Titley, S.R., Tosdal, R.M., and Wooden, J.L., 1999, Lead isotope compositions of Late Cretaceous and early Tertiary igneous rocks and sulfide minerals in Arizona: Implications for the sources of plutons and metals in porphyry copper deposits: Economic Geology, v. 94, p. 211–244.
- Caddey, S., 1999, Preliminary structural investigation, ore controls, and exploration implication of the Agua de la Falda gold deposit, Potrerillos, Chile: Minera Homestake Chile S.A. unpublished internal report, 28 p.
- Cline, J.S., Stuart, F.M., Hofstra, A.H., Premo, W., Riciputi, L., Tosdal, R.M., and Tretbar, D.R., 2003, Multiple sources of ore-fluid components at the Getchell Carlin-type gold deposit, Nevada, U.S.A.: Biennial Society for Geology Applied to Mineral Deposits Meeting, 7th, Athens, Proceedings, v. 2, p. 965–968.
- Cooke, D.R., and Simmons, S.F., 2000, Characteristics and genesis of epithermal gold deposits: Reviews in Economic Geology, v. 13, p. 221–244.
- Cornejo, P., Mpodozis, C., Ramírez, C.F., and Tomlinson, A.J., 1993, Estudio geológico de la región de Potrerillos y El Salvador (26° – 27° lat. S.): Santiago, Servicio Nacional de Geología y Minería-CODELCO registered report IR-93-01, 258 p.
- Davidson, J., and Mpodozis, C., 1991, Regional geologic setting of epithermal gold deposits, Chile: Economic Geology, v. 86, p. 1174–1186.
- Dilles, P.A., 1995, Geologic mapping of the Manto Agua de la Falda project area with technical and exploration recommendations, El Hueso mine, Chile: Minera Homestake Chile S.A. unpublished internal report, 10 p.
- Elgueta, S., and Fuentes, M., 1997, Sedimentological study of the Jurassic sequence of the area between quebradas El Asiento and El Hueso: Implications for the exploration of gold ore bodies of Jerónimo type: Minera Homestake Chile S.A. unpublished internal report, 13 p.
- Emmons, D.L., and Coyle, R.D., 1988, Echo Bay details exploration activities at its Cove gold deposit in Nevada: Mining Engineering, v. 40, p. 791–794.
- Fournier, R.O., 1985a, The behaviour of silica in hydrothermal solutions: Reviews in Economic Geology, v. 2, p. 45–62.
- 1985b, Carbonate transport and deposition in the epithermal environment: Reviews in Economic Geology, v. 2, p. 63–72.
- Gale, V.G., 1999, Characteristics and formation of the Jerónimo carbonate-replacement gold deposit, Potrerillos district, Atacama region, Chile: Unpublished M.Sc. thesis, Vancouver, University of British Columbia, 220 p.
- Gieré, R., 1996, Formation of rare earth minerals in hydrothermal systems, in Jones, A.P., Wall, F., and Williams, C.T., eds., Rare earth minerals: London, Chapman and Hall, 372 p.
- Haynes, F.M., and Kesler, S.E., 1988, Compositions and sources of mineralizing fluids for chimney and manto limestone-replacement ores in Mexico: Economic Geology, v. 83, p. 1985–1992.

- Henkelman, C., Lubben, J.D., and Cline, J.S., 2003, Variations in pyrite chemistry as clues to gold deposition at the Goldstrike system, Carlin trend, Nevada, U.S.A.: Biennial Society for Geology Applied to Mineral Deposits Meeting, 7th, Athens, Proceedings, v. 2, p. 981–984.
- Hofstra, A.H., 1994, Geology and genesis of Carlin-type gold deposits in the Jerritt Canyon district, Nevada: Unpublished Ph.D. thesis, Boulder, University of Colorado, 719 p.
- Hofstra, A.H., and Cline, J.S., 2000, Characteristics and models for Carlin-type gold deposits: Reviews in Economic Geology, v. 13, p. 163–220.
- Homestake Mining Company Annual Report, 2000, Walnut Creek, California, 60 p.
- Ilchick, R.P., 1990, Geology and geochemistry of the Vantage gold deposits, Alligator Ridge-Bald Mountain mining district, Nevada: Economic Geology, v. 85, p. 50–75.
- Kuehn, C.A., and Rose, A.W., 1995, Geology and geochemistry of wall-rock alteration at the Carlin gold deposit, Nevada: Economic Geology v. 87, p. 1697–1721.
- Lazcano, A., and Fuentes, M., 1997, Jerónimo, un nuevo depósito aurífero en el área El Hueso-Agua de la Falda: Congreso Geológico Chileno, 8th, Antofagasta, 1997, Actas, v. 2, p. 1033–1037.
- Macfarlane, A.W., Marcet, P., LeHuray, A.P., and Petersen, U., 1990, Lead isotope provinces of the central Andes inferred from ores and crustal rocks: Economic Geology, v. 85, p. 1857–1880.
- Marsh, T.M., 1997, Geochronology, thermochronology and isotope systematics of the Cu-Au and Au-Ag deposits of the Potrerillos district, Atacama region, Chile: Unpublished Ph.D. thesis, Stanford, California, Stanford University, 341 p.
- Marsh, T.M., Einaudi, M.T., and McWilliams, M., 1997, ⁴⁰Ar/³⁹Ar geochronology of Cu-Au and Au-Ag mineralization in the Potrerillos district, Chile: Economic Geology, v. 92, p. 784–806.
- Matthews, A., and Katz, A., 1977, Oxygen isotope fractionation during dolomitization of calcium carbonate: Geochimica et Cosmochimica Acta, v. 41, p. 1431–1438.
- Megaw, P.K.M., 1998, Carbonate-hosted Pb-Zn-Ag-Cu-Au replacement deposits: An exploration perspective: Mineralogical Association of Canada Short Course, v. 26, p. 337–357.
- Megaw, P.K.M., Ruiz, J., and Tittley, S.R., 1988, High-temperature, carbonate-hosted, Ag-Pb-Zn(Cu) deposits of northern Mexico: Economic Geology, v. 83, p. 1856–1885.
- Mpodozis, C., and Ramos, V., 1990, The Andes of Chile and Argentina: Circum-Pacific Council for Energy and Mineral Resources, Earth Science Series, v. 11, p. 59–90.
- Mpodozis, C., Tomlinson, A.J., and Cornejo, P., 1994, Acerca del control estructural de intrusivos eocenos y pórfidos cupríferos en la región de Potrerillos-El Salvador: Congreso Geológico Chileno, 7th, Concepción 1994, Actas, v. 2, p. 1596–1600.
- Ohmoto, H., 1986, Stable isotope geochemistry of ore deposits: Reviews in Mineralogy, v. 16, p. 491–559.
- Ohmoto, H., and Rye, R.O., 1979, Isotopes of sulfur and carbon, in Barnes, H.W., ed., Geochemistry of hydrothermal ore deposits, 2nd ed.: New York, John Wiley and Sons, p. 509–567.
- Olson, S.F., 1983, Geology of the Potrerillos district, Atacama, Chile: Unpublished Ph.D. thesis, Stanford, California, Stanford University, 190 p.
- O'Neil, J.R., Clayton, R.N., and Mayeda, T.K., 1969, Oxygen isotope fractionation in divalent metal carbonates: Journal of Chemical Physics, v. 51, p. 5547–5558.
- Prescott, B., 1926, The underlying principles of limestone replacement deposits of the Mexican province: Engineering and Mining Journal, v. 122, p. 246–253, 286–296.
- Radtke, A.S., 1985, Geology of the Carlin gold deposit, Nevada: U.S. Geological Survey Professional Paper 1267, 124 p.
- Radtke, A.S., Rye, R.O., and Dickson, F.W., 1980, Geology and stable isotope studies of the Carlin gold deposit, Nevada: Economic Geology, v. 75, p. 641–672.
- Reyes, A.G., 1990, Petrology of the Philippine geothermal systems and the application of alteration mineralogy to their assessment: Journal of Volcanology and Geothermal Research, v. 43, p. 279–309.
- Rimstidt, J.D., 1997, Gangue mineral transport and deposition, in Barnes, H.W., ed., Geochemistry of hydrothermal ore deposits, 3rd ed.: New York, John Wiley and Sons, p. 487–516.
- Seward, T.M., 1991, The hydrothermal geochemistry of gold, in Foster, R.P., ed., Gold metallogeny and exploration: Glasgow, Blackie and Son, p. 37–62.
- Simian, M.E., 2000, Geology and geochemistry of the Jerónimo gold deposit, Potrerillos district, III region, Chile: Unpublished M.Sc. thesis, Golden, Colorado School of Mines, 132 p.
- Simmons, S.F., and Christenson, B.W., 1994, Origins of calcite in a boiling geothermal system: American Journal of Science, v. 294, p. 361–400.
- Simon, G., Kesler, S.E., and Chryssoulis, S., 1999, Geochemistry and textures of gold-bearing arsenian pyrite, Twin Creeks, Nevada: Implications for deposition of gold in Carlin-type deposits: Economic Geology, v. 94, p. 405–422.
- Sillitoe, R.H., 1991a, Intrusion-related gold deposits, in Foster, R.P., ed., Gold metallogeny and exploration: Glasgow, Blackie and Son, p. 165–209.
- 1991b, Gold metallogeny in Chile—an introduction: Economic Geology, v. 86, p. 1187–1205.
- 1997, Comments on the Jerónimo gold deposit and its position in the Potrerillos district, northern Chile: Minera Homestake Chile S.A. unpublished internal report, 11 p.
- Sillitoe, R.H., and Bonham, H.F., Jr., 1990, Sediment-hosted gold deposits: Distal products of magmatic-hydrothermal systems: Geology, v. 18, p. 157–161.
- Stacey, J.S., and Kramers, J.D., 1975, Approximation of terrestrial lead isotope evolution by a two-stage model: Earth and Planetary Science Letters, v. 26, p. 207–221.
- Theodore, T.G., 2000, Geology of pluton-related gold mineralization in the Battle Mountain mining district, Nevada: Tucson, University of Arizona Press, 271 p.
- Tittley, S.R., 1991, Characteristics of high-temperature, carbonate-hosted massive sulphide ores in the United States, Mexico and Peru: Geological Association of Canada Special Paper 40, p. 585–614.
- Tomlinson, A.J., 1994, Relaciones entre el pórfido cuprífero y la falla inversa de la mina de Potrerillos: Un caso de intrusión sintectónica, Congreso Geológico Chileno, 7th, Concepción, Actas, v. 2, p. 1629–1633.
- Tomlinson, A.J., Mpodozis, C., Cornejo, P., Ramírez, C.F., and Dumitru, T., 1994, El sistema de fallas Sierra Castillo-Agua Amarga: Transpresión sinistral eocena en la Precordillera de Potrerillos-El Salvador, Congreso Geológico Chileno, 7th, Concepción, Actas, v. 2, p. 1459–1463.
- Tosdal, R.M., and Munizaga, F., 2003, Changing Pb sources in Mesozoic and Cenozoic Andean ore deposits, north-central Chile (30°–34° S): Mineralium Deposita v. 38, p. 234–250.
- Tosdal, R.M., Gibson, P.C., and Noble, D.C., 1995, Metal sources for Miocene precious-metal veins of the Orcopampa, Shila, Cailloma, and Arcata mining districts, southern Peru: Sociedad Geológica del Perú, Volumen Jubilar Alberto Benavides, p. 311–326.
- Tosdal, R.M., Wooden, J.L., and Bouse, R.M., 1999, Pb isotopes, ore deposits, and metallogenetic terranes: Reviews in Economic Geology, v. 12, p. 1–28.
- Tosdal, R.M., Cline, J.S., Fanning, C.M., and Wooden, J.L., 2003, Lead in the Getchell-Turquoise Ridge Carlin-type gold deposits from the perspective of potential igneous and sedimentary rock sources in northern Nevada: Implications for fluid and metal sources: Economic Geology, v. 98, p. 1189–1211.
- Veizer, J., and Hoefs, J., 1976, The nature of ¹⁸O/¹⁶O and ¹³C/¹²C secular trends in sedimentary carbonate rocks: Geochimica et Cosmochimica Acta, v. 40, p. 1387–1395.

